Available online at www.sciencedirect.com
ScienceDirect
Quaternary International 166 (2007) 87–110

Numerical dating of a Late Quaternary spit-shoreline complex at the northern end of Silver Lake playa, Mojave Desert, California: A comparison of the applicability of radiocarbon, luminescence, terrestrial cosmogenic nuclide, electron spin resonance, U-series and amino acid racemization methods

Lewis A. Owen[a,*], Jordon Bright[b], Robert C. Finkel[c], Manoj K. Jaiswal[d], Darrell S. Kaufman[b], Shannon Mahan[e], Ulrich Radtke[f], Joan S. Schneider[g], Warren Sharp[h], Ashok K. Singhvi[d], Claude N. Warren[i]

[a]*Department of Geology, University of Cincinnati, Cincinnati, OH 45221 0013, USA*
[b]*Department of Geology, Northern Arizona University, Flagstaff, AZ 86011, USA*
[c]*Center for Accelerator Mass Spectrometry, Lawrence Livermore National Laboratory, Livermore, CA 94550, USA*
[d]*Planetary and Geosciences Division, Physical Research Laboratory, Navrangpura, Ahmedabad 380 009, India*
[e]*United States Geological Survey, Box 25046 MS-974, Denver, CO 80225, USA*
[f]*Department of Geography, University of Köln (Cologne), Albertus-Magnus-Platz, D 50923 Köln, Germany*
[g]*Department of Anthropology, University of California, Riverside, CA 92521, USA*
[h]*Berkeley Geochronology Center, 2455 Ridge Road, Berkeley, CA 94709, USA*
[i]*Department of Anthropology and Ethnic Studies, University of Nevada, Las Vegas, NV 89154, USA*

Available online 25 January 2007

Abstract

A Late Quaternary spit-shoreline complex on the northern shore of Pleistocene Lake Mojave of southeastern California, USA was studied with the goal of comparing accelerator mass spectrometry (AMS) radiocarbon, luminescence, electron spin resonance (ESR), terrestrial cosmogenic radionuclide (TCN) surface exposure, amino acid racemization (AAR) and U-series dating methods. The pattern of ages obtained by the different methods illustrates the complexity of processes acting in the lakeshore environment and highlights the utility of a multi-method approach. TCN surface exposure ages (mostly ~20–30 ka) record the initial erosion of shoreline benches, whereas radiocarbon ages on shells (determined in this and previous studies) within the spit, supported by AAR data, record its construction at fluctuating lake levels from ~16 to 10 ka. Luminescence ages on spit sediment (~6–7 ka) and ESR ages on spit shells (~4 ka) are anomalously young relative to radiocarbon ages of shells within the same deposits. The significance of the surprisingly young luminescence ages is not clear. The younger ESR ages could be a consequence of post-mortem enrichment of U in the shells. High concentrations of detrital thorium in tufa coating spit gravels inhibited the use of single-sample U-series dating. Detailed comparisons such as this provide one of the few means of assessing the accuracy of Quaternary dating techniques. More such comparisons are needed.

1. Introduction

Quantifying rates of landscape evolution and paleoenvironmental change while establishing stratigraphic frameworks in drylands has been difficult to achieve. This is mainly because radiocarbon dating cannot be readily applied in such environments due to the lack of dateable organic material within sediments and landforms. The rapid development of alternative dating techniques (for example, terrestrial cosmogenic nuclide [TCN] surface exposure and optically stimulated luminescence [OSL]), however, is now allowing the ages of successions of sediments and landforms to be more tightly defined. Yet

*Corresponding author.
E-mail address: lewis.owen@uc.edu (L.A. Owen).

1040-6182/$ - see front matter © 2007 Elsevier Ltd and INQUA. All rights reserved.
doi:10.1016/j.quaint.2007.01.001

there are still few studies that provide comparisons between these techniques to test the validity and applicability of these rapidly evolving techniques, as well as the better calibrated and more traditional radiocarbon dating methods. To compare and to test the applicability of these techniques we applied radiocarbon, OSL, electron spin resonance (ESR), TCN surface exposure, amino acid racemization (AAR) and uranium series dating methods at a Late Quaternary spit-shoreline complex at the northern end of Sliver Lake in the Mojave Desert (Fig. 1). The site is exceptional because of the abundant radiocarbon-dated shells and tufa (Ore and Warren, 1971); hence, the site provides a radiocarbon chronology testable by other methods. Furthermore, several generations of studies of the sediment and landforms have been undertaken and therefore Silver Lake is one of the best-studied and dated Late Quaternary playa lakes in the world. Detailed studies at sites such as this will help refine geochronologic methods and will provide insights into new ways of employing numerical dating techniques to the complex and dynamic processes within arid and semi-arid environments.

2. Study site

The study site is located at the northern end of Silver Lake playa in the Mojave Desert, near the town of Baker, in San Bernardino County, California (Fig. 1). Soda and Silver Lake playas are lakebed remnants of an ephemeral Late Quaternary lake, known as Lake Mojave (Thompson, 1921, 1929; Ore and Warren, 1971; Enzel et al., 1989). The playas are fed by the Mojave River and presently flood only during extremely wet years. The study site forms part

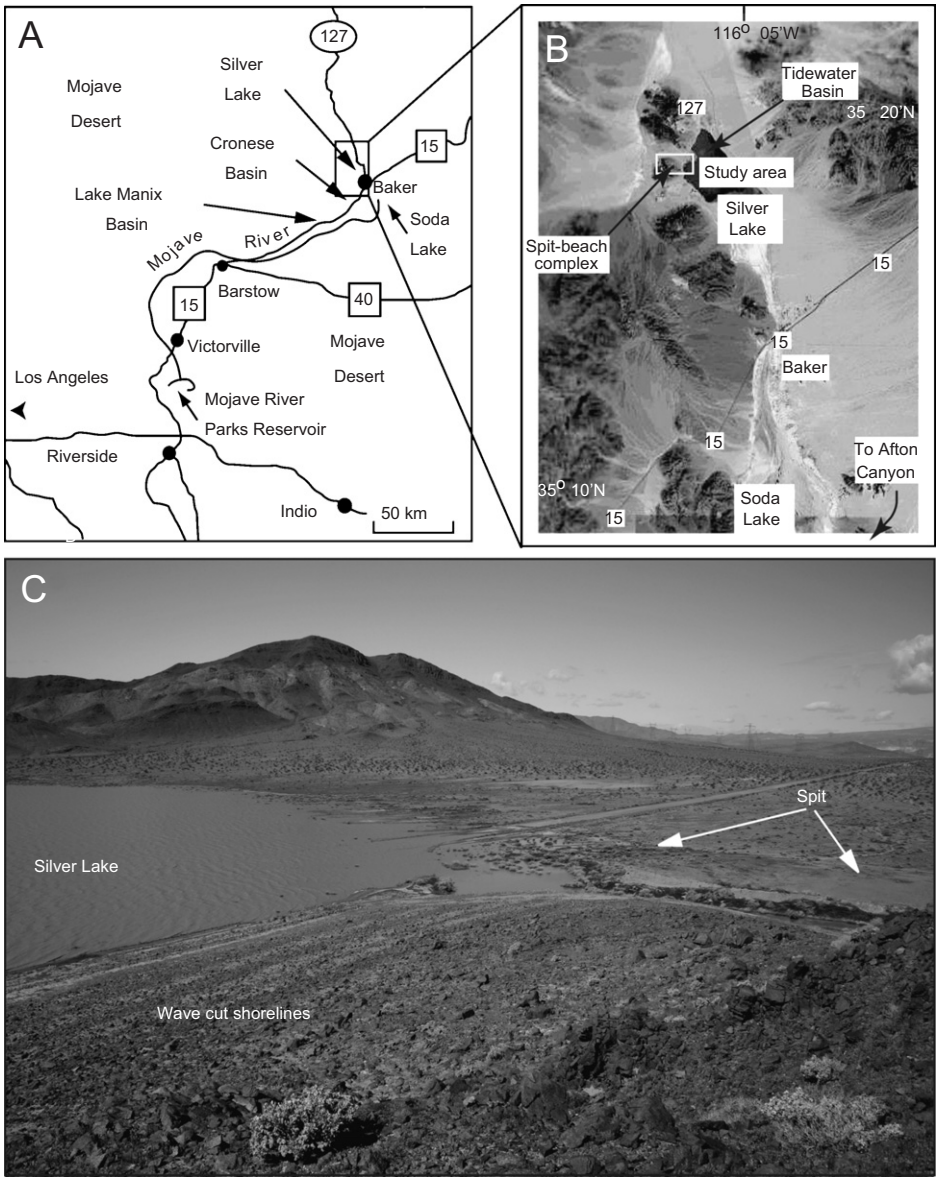

Fig. 1. (A) and (B) Location maps of study area and (C) view looking west across the spit-shoreline complex. The photograph was taken in March 2005 after an exceptionally wet winter. Silver Lake is dry most years.

of the Silver Lake basin making up the northeastern part of the Mojave Desert Block (MDB) tectonic province. The MDB is bounded by the San Andreas Fault system on its western and southern margins, by the Garlock fault on the north, and extends eastward roughly to the California–Arizona and California–Nevada borders. Locally, the Soda Mountains border the western flank of the Silver Lake basin, whereas alluvial fans form the eastern boundary (Brown, 1989).

Late Quaternary lake shorelines were identified at this site in the 1930s by archeologists (Campbell et al., 1937) who discovered artifacts associated with the shorelines. These artifacts are collectively known as the Lake Mojave Culture. In the late 1960s, archeologists (Ore and Warren, 1971; Warren and Ore, 1978) began to investigate Bench Mark Bay, which is located immediately down slope from the Lake Mojave Culture archeological site at an altitude of ~288 m above sea level (asl) as recorded by Campbell et al. (1937). Excavations in the area revealed lithic artifacts at a depth of between 15 and 29 cm. Warren and Ore (1978) collected shells of *Anodonta californiensis* (a freshwater bivalve) and calcareous tufa from a gravel quarry southwest of Bench Mark Bay and obtained 24 ages using the then newly developed technique of radiocarbon dating developed in the 1950s. On the basis of the stratigraphy and the radiocarbon dating, Ore and Warren (1971) suggested that there were four high stands of Lake Mojave during the Late Pleistocene to Early Holocene: the first ended at around 17.5 ka, and subsequent high stands occurred approximately from 16.4 to 13.8, 12.9 to 10.2 and 9.5 to 8.4 ka. In this paper, all radiocarbon ages are calibrated using OxCal with the calibration curves of Reimer et al. (2004) unless otherwise stated. Finally, Ore and Warren (1971) associated the cultural materials with geological units.

More recent studies on the Late Quaternary geology and paleohydrology of Lake Mojave by Brown (1989) and Wells et al. (2003) provide a complex history of lake-level fluctuations recorded in cored lake deposits and associated shoreline features. Their work suggested that episodic flooding of the basin began around 22 ka with prolonged high stands lasting between 2000 and 3000 years. Two major high and persistent lake stands occurred in the Silver Lake basin (and presumably in the Soda Lake basin), between ~18.4 and 16.6 ka (Lake Mojave I) and 13.7 and 11.4 ka (Lake Mojave II). Furthermore, they suggested these pluvial periods resulted from significantly increased precipitation and annual large-scale floods (Enzel et al.,

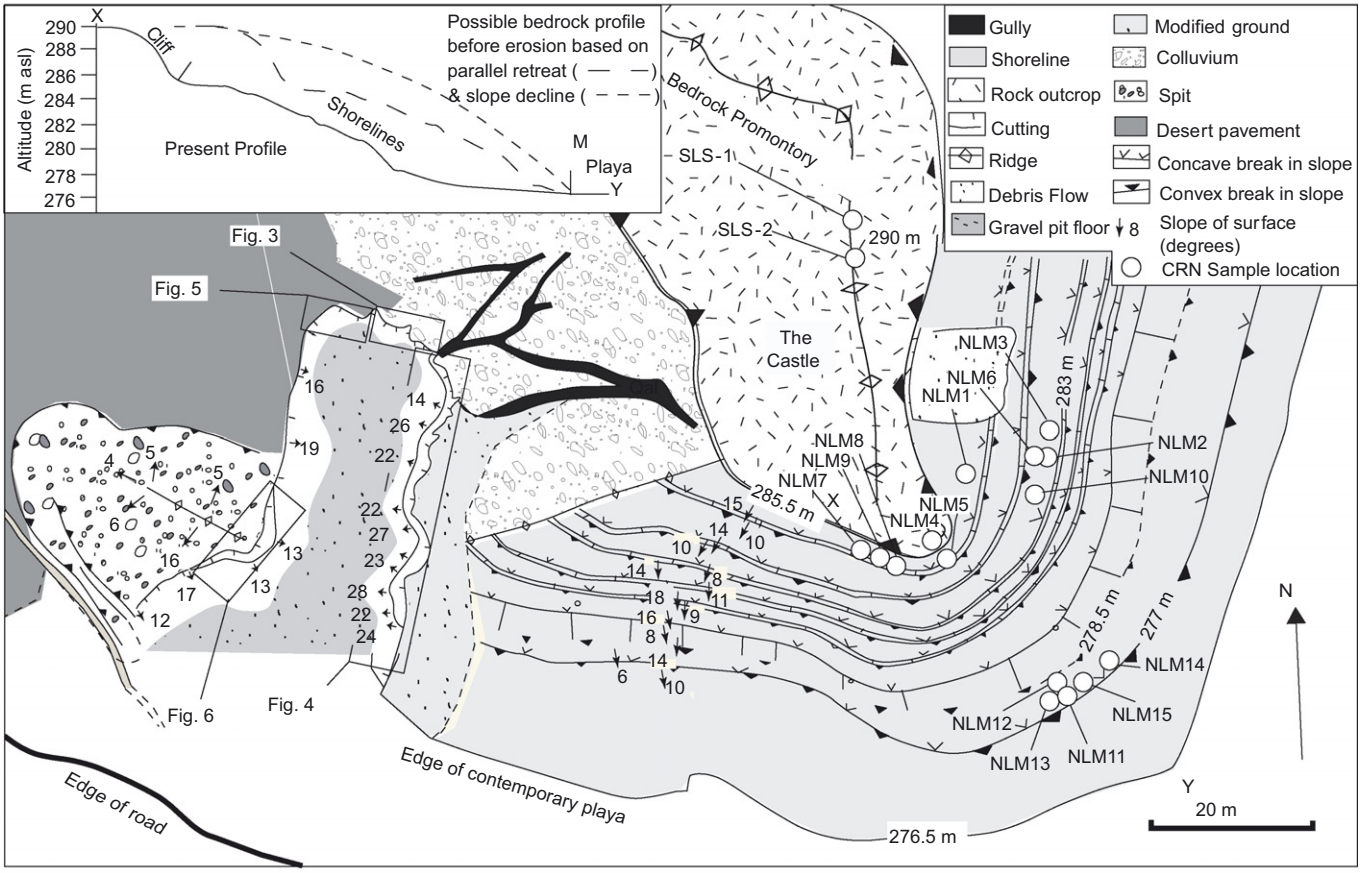

Fig. 2. Site map of the spit-shoreline complex study area. Silver Lake Quarry is located in the eastern part of the map. The inset shows the present profile from the top of cliff (*X*) to the contemporary playa (*Y*) showing hypothetical cliff profiles before erosion by either parallel retreat or slope decline (see text for full discussion).

1989). The average annual flow in the lower reaches of the Mojave River needed to form and maintain Silver Lake (or any other lake that was part the Mojave Drainage system) would have had to been at least an order of magnitude larger than the present-day average discharge (Enzel et al., 2003b). Periods of intermittent lake conditions, during which the Silver Lake basin experienced several desiccation events, separated the higher stands and more continuous Lake Mojave phases. The most significant drying event is recorded by large desiccation cracks in core sediments filled with windblown sand at ~18–19 ka.

Wells et al. (2003) suggested that Lake Mojave I stabilized to form a shoreline at 287–288 m asl (A-shoreline). They suggested that Lake Mojave II was coincident with the incision of Afton Canyon and subsequent draining of Lake Manix. This event was associated with increased sediment loading and likely resulted in significantly greater overflow of Lake Mojave into the Death Valley basin. The overflow produced controlled incision of the Lake Mojave outlet spillway between 13 and 14 ka, and ultimately stabilizing at an elevation of 285.5 m (B-shoreline). However, the spillway may have been initially cut prior to 14 ka (Y. Enzel, pers. commun.). Wells et al. (2003) emphasized that the majority of shoreline features around the margins of Silver and Soda lakes date to Lake Mojave II, as the shallow lake conditions resulted in modification and erosion of older Lake Mojave I landforms. A transition to a drier climatic regime resulted in the total drying of Lake Mojave by ~9.7 ka, with playa conditions dominating Silver Lake and Soda Lake basins following this time.

Our study site comprises a spit and associated shorelines that have been quarried at the northwestern end of Silver Lake (Figs. 1 and 2). Wells et al. (2003) called this site "Silver Lake quarry" and argued that the top of this quarry is ~8 m below A-Shoreline, which is preserved as a wave-cut cliff in the dioritic bedrock flanking the quarry.

The previously determined radiocarbon ages preserve stratigraphic order from the oldest (unit 1 — 16.2 ± 0.9 ka) to the youngest unit (unit 10 — 9.2 ± 0.5 ka; Ore and Warren, 1971). Wells et al. (2003) suggested that there are two stratigraphic packages within the spit (unit a and units b–i) separated by a sharp contact. The lower stratigraphic package (unit a, undated) comprises predominately weathered angular to subrounded pebbles and cobbles. The upper package (units b–i) has yielded calibrated radiocarbon ages ranging from ~16 to 10 ka and comprises alternating layers of silty clay, sand, and unweathered gravel along the flanks of the spit. Wells et al. (2003) suggested that the difference in weathering of the two packages of sediment indicates a significant hiatus in deposition of the two units. They suggested that the base of the spit therefore predates ~16 ka, and that these deposits were exposed subaerially during lake-lowering events to allow the weathering of clasts, which was probably enhanced by salts derived from the lake. Wells et al. (2003) and Jefferson (2003) described ostracode faunas in

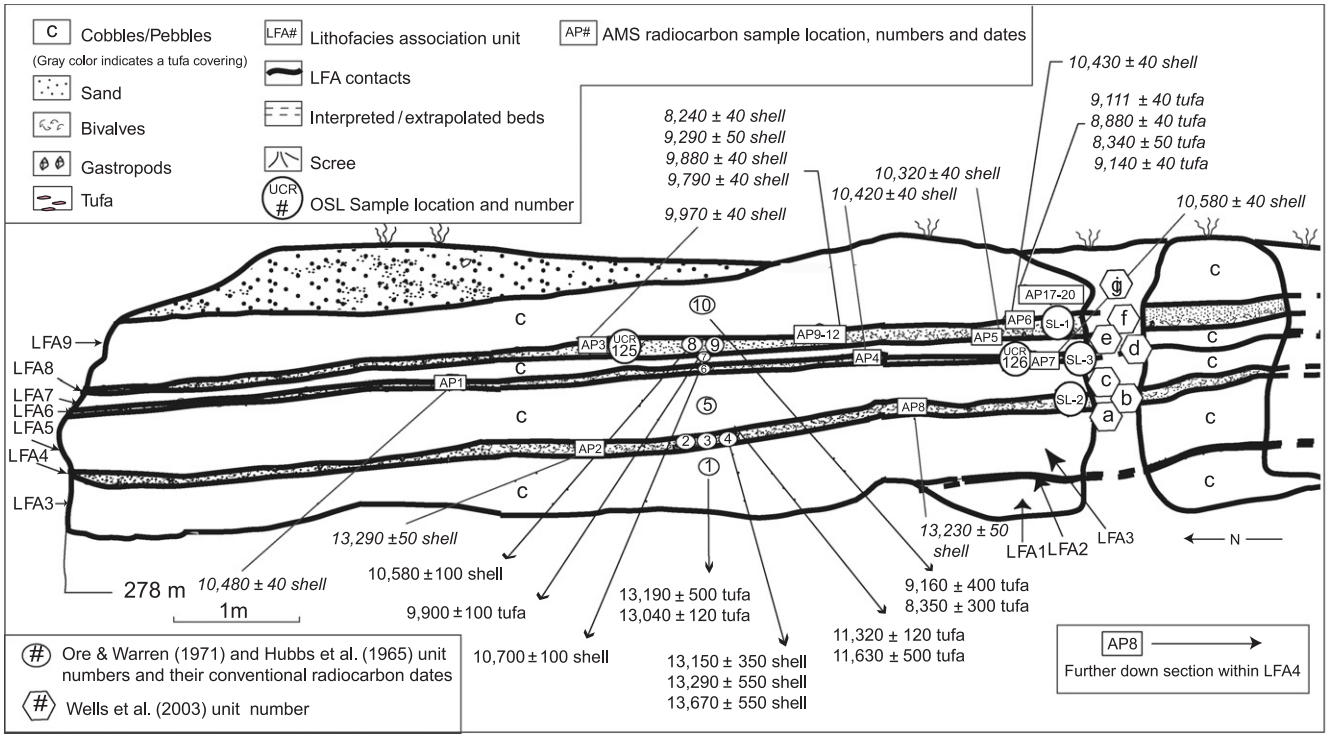

Fig. 3. Section at the northern end of Silver Lake quarry showing the positions for the luminescence and radiocarbon samples, and each of the sedimentary units. The uncalibrated conventional and accelerator mass spectrometry radiocarbon ages are plotted (see Fig. 2 for location). LFA–lithofacies association.

sediments throughout Lake Mojave and Lake Manix to provide a proxy for paleoenvironmental conditions during the Late Quaternary.

3. Field methods

The site was mapped at a scale of 1:1000 using a plane table aided by the use of differential global positioning system technology (Fig. 2). The mapping shows a succession of shorelines cut into bedrock rising to a >3-m-high wave-cut cliff of a bedrock promontory. A small sandy spit is present on the western side of the study area, which has been excavated for gravel, forming a large pit (Fig. 2). This ridge represents a small spit that derived much of its sediment from the southern and eastern shorelines at the base of the promontory. The spit sheltered an area of slackwater behind it and to the north.

Sections within the gravel quarry were logged using leveling and the standard methods of Evans and Benn (2004). Both lateral and vertical graphic sedimentary logs were constructed (Figs. 3–6). Similar sediments within the sections were grouped into lithofacies associations (LFAs). The units of Ore and Warren (1971) and Wells et al. (2003), which do not correspond exactly with our LFAs, are shown in Fig. 3 for comparison. Samples were collected for accelerator mass spectrometry (AMS) radiocarbon, OSL, ESR, TCN surface exposure, AAR and U-series dating and for ostracode fauna analysis. These are described in detail in the next section.

4. Results

4.1. Ostracode faunas

Ostracode faunas were recovered from LFA 2, 4, 6 and h (Table 1; corresponding to fine grained units b, d, f and h from Fig. 12 of Wells et al., 2003). The assemblages comprise dominantly, and most importantly, *Limnocythere ceriotuberosa*. This ostracode taxon has been interpreted as a lacustrine-facies indicator and has been reported from numerous fossil localities from Lake Mojave and Lake Manix sediment localities (e.g., Wells et al., 2003; Jefferson, 2003). In comparison, ostracode assemblages from the Tidewater basin area at the northeastern extent of Silver Lake (Fig. 1B) contain both *L. ceriotuberosa* and *L. bradburyi* (Wells et al., 2003). While not definitive, the dating of sediment in the Tidewater basin indicates that *L. ceriotuberosa* and *L. bradburyi* coexist in deposits older than ~18.5±0.6 ka (specifically units IV and VI of Wells et al., 2003; correlating with Lake Mojave I) whereas *L. ceriotuberosa* has been recovered from sediments younger than approximately 15.8±0.5 ka (unit VIII and possibly XI, although unit XI has not been dated; correlating with Lake Mojave II). When combined with the Tidewater basin chronology, the dominance of *L. ceriotuberosa* and the absence of *L. bradburyi* in all of the fine-grained sedment from Silver Lake quarry suggest that the spit sediments was deposited during Lake Mojave II or later. This also suggests that the undated,

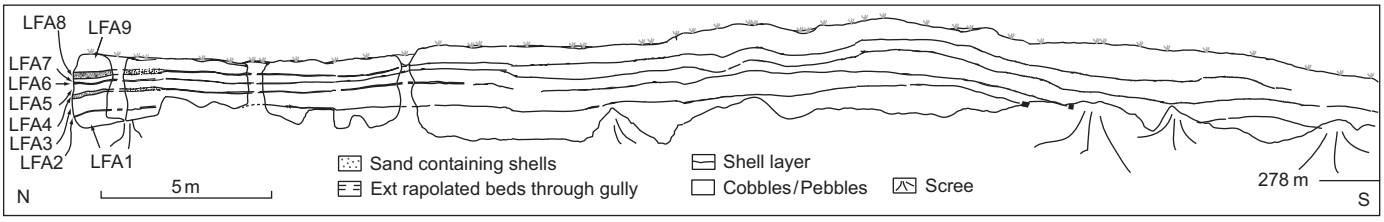

Fig. 4. Section through the main spit at Silver Lake quarry (see Fig. 2 for location).

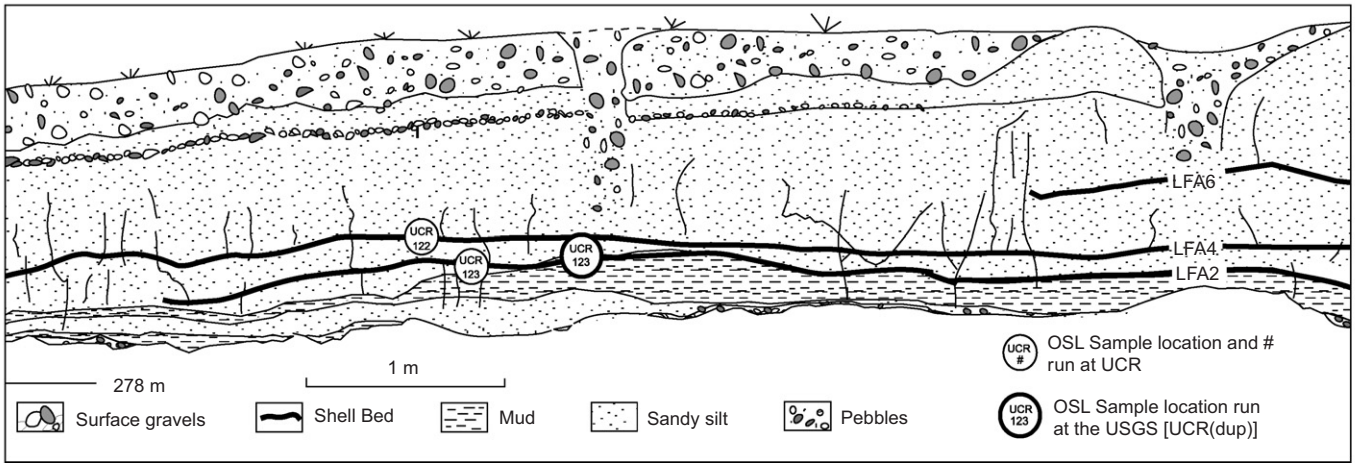

Fig. 5. Section at the northwestern end of Silver Lake quarry (see Fig. 2 for location).

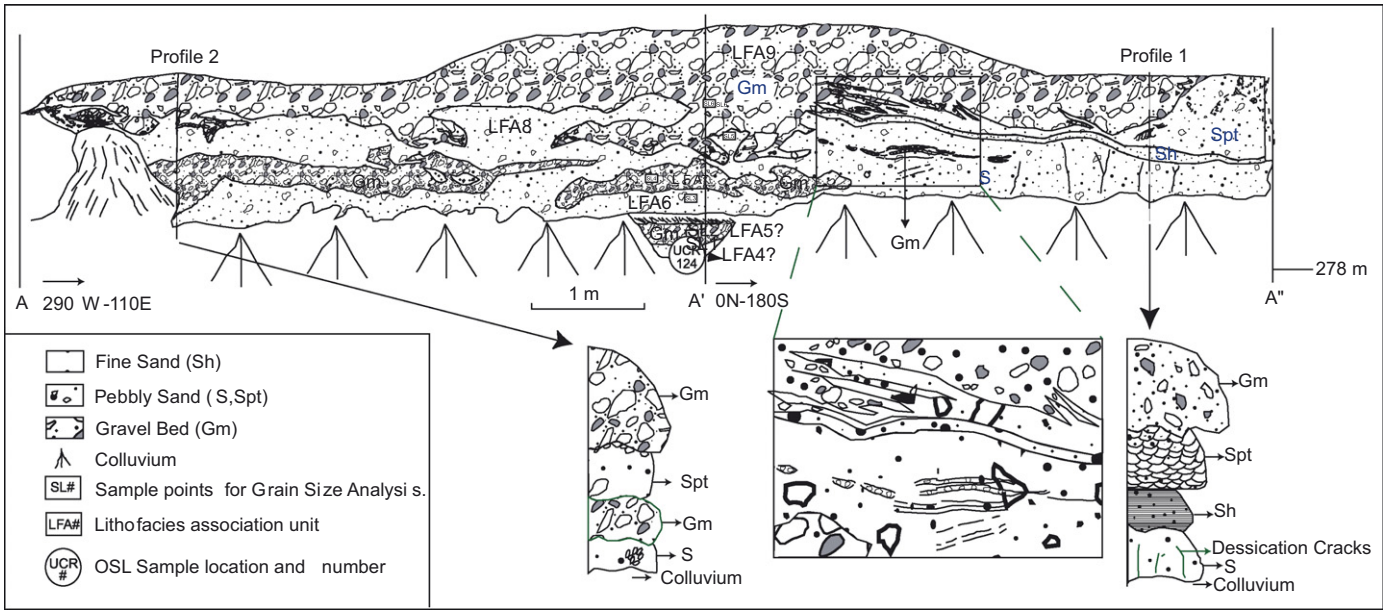

Fig. 6. Section at the western end of Silver Lake quarry (see Fig. 2 for location).

Table 1
Ostracode fauna from Silver Lake Quarry

Sample[a]	Ostracode fauna[b]	Juveniles
(h)	*Limnocythere ceriotuberosa*	No
LFA 8 (f)	*Limnocythere ceriotuberosa*	No
LFA 6 (d)	*Limnocythere ceriotuberosa*; *Heterocypris incongruins*	Yes
LFA 4 (b)	*Limnocythere ceriotuberosa*; *Candona* sp. 1; *Candona* sp. 2 *Heterocypris incongruins*; *Cypridopsis vidua*	Yes

[a]LFA units match designations on Fig. 3 (this paper), bracketed letter matches unit designation from Fig. 12 in Wells et al. (2003).
[b]Ostracode valves were not counted. Species are ranked in order of declining estimated abundance.

L. ceriotuberosa-bearing, fine-grained unit at the base of the Silver Lake quarry (LFA 4 or b; Fig. 3) may be older than 15.8 ka, which is in agreement with the three overlying radiocarbon ages from LFA 3 that are ~15.8 ka (or unit a from Fig. 12 in Wells et al., 2003).

The ostracode assemblages (Table 1) suggest that reworking of sediment within units LFA 4 and LFA 6 is minor because both adult and juvenile valves are present. Only adult ostracodes were recovered from LFA 8 and unit h of Wells et al. (2003), which probably suggests that a small amount of reworking or winnowing has removed the smaller ostracode valves.

4.2. Radiocarbon dating

Radiocarbon samples (AP13–AP15: Table 2) were also collected from three locations in the Cronese basin, ~15 km west of Lake Mojave, where *A. californiensis* shells and charcoal occur within the same archeological features (Fig. 1). This is one of the rare locations where both charcoal and shells can be found together. The two Cronese basin lakes are integral parts of the Mojave River drainage system; these lakes are also filled episodically by flood waters of the river in the same way as Lake Mojave (i.e., present day Silver Lake and Soda Lake playas). Because the source catchment for the water is also the same, we reasoned that shells from the Cronese basin were influenced by the same hardwater effect as shells in the Silver Lake basin. Paired charcoal-shell samples collected from the Cronese basin were used to investigate reservoir corrections for the Silver Lake gravel quarry sections because charcoal was not found at the Silver Lake site. The AMS radiocarbon ages for paired samples of *A. californiensis* and charcoal are shown in Fig. 7A. These do not show a large difference in age (<150 years) between the charcoal and shell radiocarbon ages. Although samples AP13–AP15 suggest no significant hardwater effect for *A. californiensis* shells in the Cronese basin, we cannot rule out the possibility that hardwater effects may have producing older ages for Mojave Lake. Our results are compatible with those of Berger and Meek (1992) who analyzed live, pre-atmospheric nuclear testing *A. californiensis* from the Mojave River system, which showed that the hardwater effect on *A. californiensis* in the Mojave River basin is ~450 years. They also compared radiocarbon ages on *A. californiensis* with other materials, and assessed the internal stratigraphic consistency of the radiocarbon ages. However, their samples were from two different sites, so direct application of the hardwater effect that they estimated to our results is difficult to fully assess.

Table 2
AMS radiocarbon dates

Sample ID	Lab ID (CAMS)	Material dated	LFA	$\delta^{13}C$ (‰)[a]	Fraction modern	$D^{14}C$	^{14}C years BP	Calibrated years BP (95.4% probability using OxCal)
AP1	76411	*Anodonta californiensis* shell	6	−5	0.2713±0.0013	−728.7±1.3	10480±40	12680–12230
AP2	76412	*Anodonta californiensis* shell	4	−5	0.1913±0.0010	−808.7±1.0	13290±50	16150–15400
AP3	76413	*Anodonta californiensis* shell	8	−5	0.2889±0.0012	−711.1±1.2	9970±40	11620–11250
AP4	76414	*Anodonta californiensis* shell	6	−5	0.2734±0.0013	−726.6±1.3	10420±40	12410–12100
AP5	76415	*Anodonta californiensis* shell	8	−5	0.2768±0.0012	−723.2±1.2	10320±40	12380–11980
AP6	76416	*Anodonta californiensis* shell	8	−5	0.2731±0.0013	−726.9±1.3	10430±40	12620–12120
AP7	76417	*Anodonta californiensis* shell	6	−5	0.2679±0.0013	−732.1±1.3	10580±40	12790–12390
AP8	76418	*Anodonta californiensis* shell	4	−5	0.1926±0.0010	−807.4±1.0	13230±50	16050–15300
AP9	76419	*Anodonta californiensis* shell	8	−5	0.3586±0.0017	−641.4±1.7	8240±40	9410–9030
AP10	76420	*Anodonta californiensis* shell	8	−5	0.3146±0.0016	−685.4±1.6	9290±50	10650–10280
AP11	76421	*Anodonta californiensis* shell	8	−5	0.2922±0.0014	−707.8±1.4	9880±40	11400–11210
AP12	76422	*Anodonta californiensis* shell	8	−5	0.2957±0.0014	−704.3±1.4	9790±40	11260–11170
AP13A	76423	*Anodonta californiensis* shell	n/a	−5	0.9039±0.0043	−96.1±4.3	810±40	800–670
AP13B	76487	Charcoal[b]	n/a	−25	0.9151±0.0051	−84.9±5.1	710±50	740–550
AP14A	76424	*Anodonta californiensis*	n/a	−5	0.8999±0.0046	−100.1±4.6	850±50	910–680
AP14B	76488	Charcoal[b]	n/a	−25	0.9214±0.0041	−78.6±4.1	660±40	680–550
AP15A	76425	*Anodonta californiensis*	n/a	−5	0.9046±0.0035	−95.4±3.5	810±40	800–670
AP15B	76489	Charcoal[b]	n/a	−25	0.8982±0.0052	−101.8±5.2	860±50	920–680
AP16	76426	*Anodonta californiensis*	n/a	−5	0.2884±0.0014	−711.6±1.4	9990±40	11700–11260
AP17	76427	Tufa	9	−5	0.3216±0.0016	−678.4±1.6	9110±40	10390–10200
AP18	76428	Tufa	9	−5	0.3310±0.0016	−669.0±1.6	8880±40	10180–9780
AP19	76429	Tufa	9	−5	0.3543±0.0018	−645.7±1.8	8340±50	9480–9140
AP20	76430	Tufa	9	−5	0.3205±0.0013	−679.5±1.3	9140±40	10420–10220

[a]Delta ^{13}C values are the assumed values according to Stuiver and Polach (1977). Sample preparation backgrounds have been subtracted, based on measurement of samples of ^{14}C-free coal. Backgrounds were scaled relative to sample size.
[b]Samples collected from Cronese Basin.

Samples of *A. californiensis* shell and tufa were collected from sections within the Silver Lake gravel quarry (Fig. 3). Some of the *A. californiensis* shells are articulated suggesting that the shelly deposits represent life assemblages.

The shells and charcoal samples were cleaned and processed at the Center for Accelerator Mass Spectrometer in the Lawrence Livermore National Laboratory. Table 2 shows the results of the AMS radiocarbon dating. The combined calibrated conventional radiocarbon ages of Ore and Warren (1971) and the new AMS radiocarbon ages are plotted as probabilities and corrected using Bayesian analysis using the methods of BCal (http://bcal.sheffield.ac.uk/) with the calibration curves of Reimer et al. (2004; Fig. 7B).

The conventional radiocarbon ages of Ore and Warren (1971) and our new AMS ages are not significantly different (Fig. 3). This agreement provides confidence that both the original ages of Ore and Warren (1971) and our ages are accurate. The consistency of the ages derived from combined shell samples (for conventional radiocarbon) and AMS ages on single valves supports the view that the shell deposits are life assemblages and were not reworked shells. The Bayesian analysis more strongly defines the radiocarbon ages of LFA3 to LFA9, suggesting three major stages: LFA3 and LFA4 = ~16.2–~15.3 ka; LFA5 to LFA8 = ~13.3–~11.6 ka (with multiple events); and LFA9 = ~10.2–~9.9 ka. The radiocarbon ages for LFA5 to LFA8 show that these units formed during the Younger Dryas Stade.

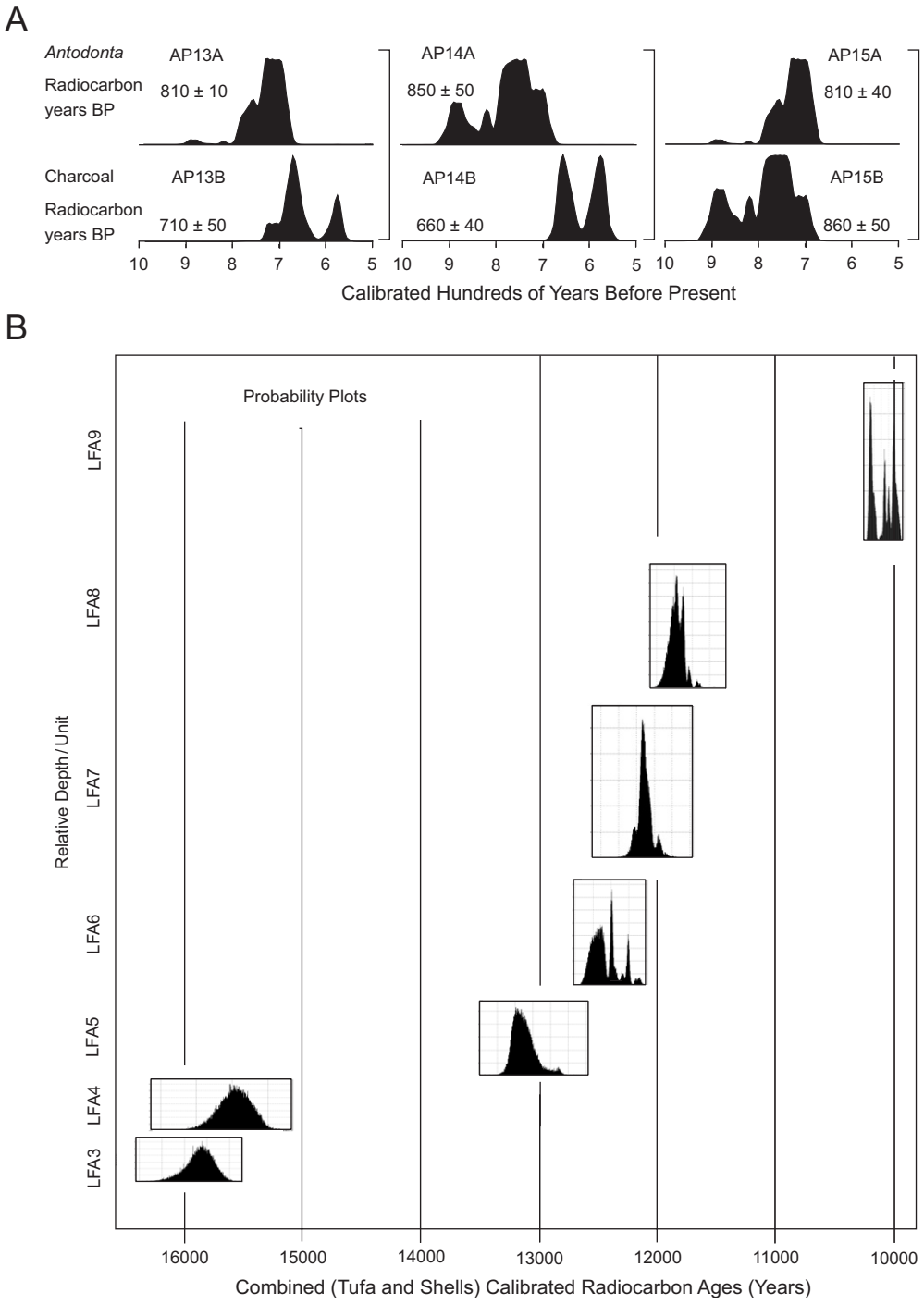

Fig. 7. Plots of calibrated radiocarbon ages. (A) Calibrated AMS radiocarbon ages BP for paired samples of *Antadonta californiernsis* and charcoal taken from the same sedimentary horizons from the Cronese basin ~15 km west of Lake Mojave shown as Gaussain probability distributions (calibrated using OxCal). (B) Calibrated radiocarbon ages BP (calibrated using OxCal) plotted as probabilities and corrected using Bayesian analysis of BCal (http://bcal.sheffield.ac.uk/) with the calibration curves of Reimer et al. (2004). All samples listed in Table 2 and in Ore and Warren (1971) were used in the Bayesian analysis.

4.3. ^{10}Be and ^{26}Al cosmogenic radionuclide surface exposure dating

The samples for TCN analysis were collected from boulders marking the highest, an intermediate and the lowest shorelines (Figs. 2 and 8). Two bedrock samples (SLS-1 and SLS-2) were also collected from the top of the promontory above the shorelines to provide estimates on the erosion rates at the site (Fig. 2). Most of the rocks that were sampled were wind polished, suggesting a moderate degree of post-lake erosion, although some sheltered rock outcrops had well developed rock varnish. Using a hammer

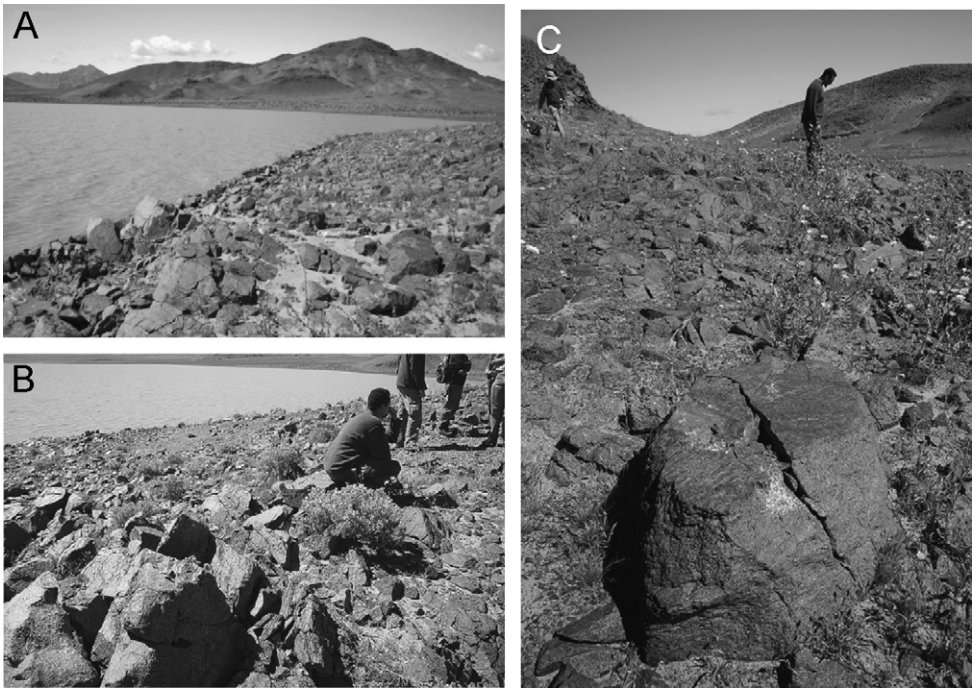

Fig. 8. Views of sampling sites for terrestrial cosmogenic surface exposure dating. (A) Wave-cut bedrock on the lowest shoreline. (B) Bedrock on the intermediate (middle) shoreline. (C) Boulder on the upper shoreline.

and chisel, samples were carved off the top (<5 cm depth) of the rock surface. Care was taken in selecting rocks that had not been recently moved and were not excessively weathered. The dioritic rocks at this location had very little quartz (<10%) and therefore we obtained about 1000 g of rock for each sample.

The samples were prepared in the geochronology laboratories at the University of California, Riverside.[1] First, the samples were crushed and sieved. Quartz was then separated from the 250–500 μm size fraction using the method of Kohl and Nishiizumi (1992). After addition of Be and Al carriers, Be and Al were separated and purified by ion exchange chromatography and precipitation at pH > 7. The hydroxides were oxidized by ignition in quartz crucibles. Then, BeO was mixed with Nb metal and Al_2O_3 with Ag metal and loaded onto targets for the determination of the $^{10}Be/^{9}Be$ and $^{26}Al/^{27}Al$ ratios by AMS at the Center for Accelerator Mass Spectrometry in the Lawrence Livermore National Laboratory. Isotope ratios were compared to ICN ^{10}Be and NIST ^{26}Al standards (Nishiizumi, 2004) and ICN ^{10}Be standards (K. Nishiizumi, pers. commun. 1995) using a ^{10}Be half-life of 1.5×10^6 yr.

The measured isotope ratios were converted to TCN concentrations in quartz using the total Be and Al in the samples and the sample weights. Radionuclide concentrations were then converted to zero-erosion exposure ages using the scaling method of Stone (2000) and a sea-level, high-latitude production rate of 5.44 atoms ^{10}Be per gram of quartz per year and were corrected for geomagnetic field variations as described in Farber et al. (2005). The production rate for ^{10}Be and ^{26}Al are presently the subject of much research; its value is likely to be more accurately defined in the coming years. However, revised production rates are not likely to change our calculated ages by more than about 5% of the age were determined. The correction for variations in the geomagnetic field is still uncertain. We therefore present the ages for samples NLM1 to NLM15 with and without the geomagnetic correction (Table 3).

We use the following equation (Lal, 1991) to approximate the steady-state erosion rate for the two bedrock samples (SLS-1 ad SLS-2) collected from the top of the promontory:

$$\varepsilon = 1/\mu(P/N - \lambda), \quad (1)$$

where ε is the steady-state boulder erosion rate (cm yr^{-1}), μ the cosmic ray absorption coefficient $= \rho/\Lambda$ (where ρ the density of rock (2.8 g cm^{-3}) and Λ the cosmic ray absorption mean free path for the boulder surface (160 g cm^{-2}) (Nishiizumi et al., 1993), P the ^{10}Be production rate at the sample location (Stone, 2000), N the measured concentration of ^{10}Be in sample (atoms g^{-1} quartz), and λ the decay constant of ^{10}Be (yr^{-1}) $= \ln 2/t_{\frac{1}{2}} = 4.62 \times 10^{-7}$ yr^{-1} (where $t_{\frac{1}{2}}$ (half-life of ^{10}Be) $= 1.5 \times 10^{-6}$ yr^{-1}).

Erosion rates determined from samples SLS-1 and SLS-2 are 3.9 and 5.1 mMa^{-1}, respectively. Using the mean of these data (4.5 mMa^{-1}) we have calculated the ages of samples NLM1–NLM15 (Table 3). These results are consistent with the view that the rocks have experienced

[1]The geochronology laboratories at the University of California, Riverside were moved to the University of Cincinnati in 2004.

Table 3
Terrestrial cosmogenic nuclide surface exposure data and ages

Sample ID	Sample type	Altitude (m asl)	Latitude/ longitude	Latitude/ altitude correction	Shielding correction	^{10}Be concentration (10^5 atoms/g)	^{26}Al concentration (10^6 atoms/g)	^{10}Be age with zero erosion (ka)	^{10}Be age geomagnetically corrected with zero erosion (ka)	^{10}Be age corrected for 4.5 m/Ma erosion, but no correction for the geomagnetic field variations (ka)	^{26}Al age (ka)	^{26}Al age geomagnetically corrected (ka)	^{26}Al age corrected for 4.5 m/Ma erosion, but no correction for the geomagnetic field variations (ka)
SLS-1	Bedrock	290.00	35°21.87′N 116°08.79′W	1.14	0.99	8.01±0.19	Not measured	141.8±3.3	129.4±3.1		—		
SLS-2	Bedrock	290.00	35°21.87′N 116°08.79′W	1.14	0.99	6.37±0.16	Not measured	112.0±2.8	103.4±2.6		—		
NLM1	Bedrock	284.41	35°21.87′N 116°08.79′W	1.13	0.99	2.16±0.06	1.20±0.09	37.6±1.0	35.5±0.9	42.7±1.2	34.4±2.6	32.7±2.5	38.7±2.9
NLM2	Bedrock	283.71	35°21.87′N 116°08.79′W	1.13	0.99	2.01±0.08	1.10±0.06	34.9±1.3	33.1±1.30	39.2±1.5	31.3±1.6	29.9±1.5	34.8±1.8
NLM3	Bedrock	283.71	35°21.87′N 116°08.79′W	1.13	0.99	1.98±0.07	1.08±0.08	34.4±1.1	32.7±1.1	38.7±1.3	30.8±2.2	29.5±2.1	34.2±2.5
NLM4	Bedrock	284.95	35°21.87′N 116°08.79′W	1.13	0.99	1.31±0.07	0.74±0.05	22.7±1.2	22.0±1.1	24.4±1.2	20.9±1.5	20.4±1.4	22.4±1.6
NLM5	Boulder	284.41	35°21.87′N 116°08.79′W	1.13	0.99	1.33±0.07	0.82±0.05	23.0±1.1	22.3±1.1	24.8±1.2	23.4±1.5	22.8±1.4	25.3±1.6
NLM6	Boulder	283.8	35°21.87′N 116°08.79′W	1.13	0.99	1.51±0.08	0.92±0.06	26.1±1.3	25.2±1.3	28.5±1.5	26.2±1.6	25.3±1.6	28.6±1.8
NLM7	Boulder	283.37	35°21.87′N 116°08.79′W	1.13	0.99	1.60±0.08	0.89±0.05	27.8±1.4	26.8±1.3	30.5±1.5	25.3±1.5	24.5±1.4	27.6±1.6
NLM8	Boulder	283.37	35°21.87′N 116°08.79′W	1.13	0.99	1.46±0.06	0.86±0.06	25.3±1.0	24.5±0.9	27.5±1.1	24.5±1.6	23.7±1.6	26.5±1.8
NLM9	Boulder	283.37	35°21.87′N 116°08.79′W	1.13	0.99	1.21±0.07	0.69±0.04	21.0±1.2	20.5±1.1	22.4±1.2	19.5±1.0	19.1±1.0	20.8±1.1
NLM10	Bedrock	283.8	35°21.87′N 116°08.79′W	1.09	0.99	1.28±0.05	0.76±0.05	23.0±1.0	22.3±0.9	24.8±1.0	22.3±1.5	21.8±1.5	24.1±1.6
NLM11	Bedrock	278.44	35°21.87′N 116°08.79′W	1.13	0.99	2.60±0.08	1.32±0.08	45.5±1.5	42.2±1.3	53.5±1.7	38.0±2.3	35.9±2.1	43.4±2.6
NLM12	Bedrock	278.44	35°21.87′N 116°08.79′W	1.13	0.99	1.67±0.08	0.95±0.08	29.1±1.0	27.9±1.0	32.1±1.1	27.3±2.4	26.3±2.3	29.9±2.6
NLM13	Bedrock	278.44	35°21.87′N 116°08.79′W	1.13	0.99	2.01±0.06	1.25±0.06	35.0±1.0	33.2±1.0	39.5±1.2	36.0±1.8	34.1±1.7	40.8±2.0
NLM14	Bedrock	278.44	35°21.87′N 116°08.79′W	1.13	0.99	1.31±0.05	Not measured	22.7±0.9	22.1±0.9	24.5±1.0	—		
NLM15	Bedrock	278.44	35°21.87′N 116°08.79′W	1.13	0.99	1.58±0.06	Not measured	27.5±1.1	26.5±1.1	30.2±1.2	—		

moderate erosion possibly due to eolian processes. The spread of TCN ages is considerable, ranging from >50 to ~20 ka (Fig. 9). There is no significant difference between ages for all the shorelines (the means of each dataset is within one standard deviation of that of the other datasets). The spread of ages may be attributed to three main factors.

Firstly, young ages may reflect erosion of bedrock surfaces and boulders, or toppling of boulders that has exposed new surfaces. We account for erosion by incorporating the 4.5 mMa^{-1} erosion rate. The effect of this is most significant for the older samples. To minimize the likelihood of toppling of boulders, we chose the most stable boulders on each surface, which include ones that were well inset into the substrate and large tabular ones that were not precarious.

Secondly, the old ages might reflect inheritance of TCNs within bedrock surfaces if the bedrock had not been sufficiently eroded to expose rock that was previously shielded from cosmogenic rays. We are not able to accurately reconstruct the shape of the promontory before its erosion. However given that the present cliff is between 3 and 5 m high and that rock crops out to the present day playa surface, we have reconstructed likely maximum (highest) former profiles based on slope decline and parallel retreat of the cliff (inset in Fig. 2). To be conservative, and using a cliff height of 3 m, we would expect ~2% production of TCN in bedrock that was originally shielded by 3 m of rock. Greater rock thicknesses, as implied by our reconstruction shown in Fig. 2, would reduce the production rate even further. Given that samples on the top of the headland (SLS-1 and SLS-2) suggest that the bedrock surface may be significantly older than 140 ka, and using a conservative estimate of former rock thickness (3 m), then we might expect at least 2 ka years of inheritance, and possibly significantly more. Since the initial topography prior to the erosion of the headland is unknown, it may have been very irregular, and this might explain the lack of a systematic ages progression among the shorelines.

Thirdly, the shorelines may have been covered with sediment and were likely covered by the lake water for a significant period during each high stand. This would have shielded the surfaces from cosmic rays resulting in younger ages. The shorelines probably were not covered by sediment for any significant time because their original morphology appears to be preserved. However, changes in the lake level at this location may have had a significant impact on the production rates within the rock surfaces. For example, a water depth of 10 m (an approximate maximum depth before the lake would overspill) can reduce the production rate of ^{10}Be by ~90%. Enzel et al. (2003b) estimated that Lake Mojave likely was filled for

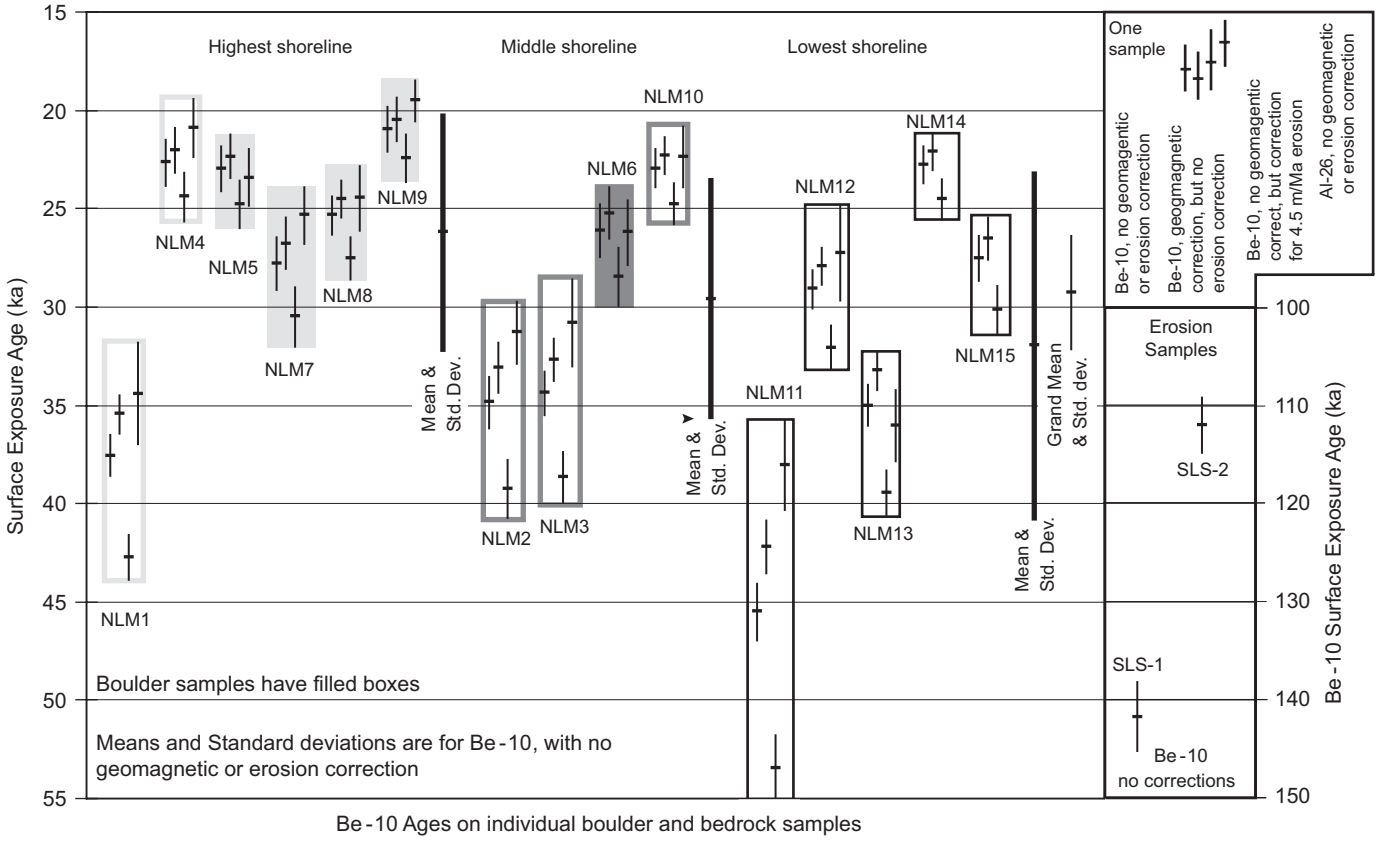

Fig. 9. Terrestrial cosmogenic nuclide surface exposure data plotted by for the highest, middle and lowest shorelines, and for the bedrock samples collected from the top of the promontory. The mean values for each shoreline do not include corrections for variations in the geomagnetic field or erosion.

about 50% of its duration during the Late Glacial. This would clearly have reduced the production of ^{10}Be and resulting in younger TCN ages.

All of these factors complicate the interpretations of the TCN on the shorelines. Nevertheless, TCN ages appear to cluster between about 20 and 35 ka, suggesting that the TCN age of the shorelines is between 20 and 35 ka, given a few thousand years of likely inheritance. The weighted mean of the spread of ages near the cliff, which would have been under the greatest cover of rock and best shielded to have little inherited TCNs, is ~24–25 ka. Given 2000–4000 years of possible inheritance the shoreline may be as young as 20 ka. However, given the likely cover of the shorelines by water during high lake stands and possible sediment cover, which would shield the bedrock and reduce the TCN ages, we therefore favor a TCN age of between 20 and 25 ka for the shorelines.

4.4. Luminescence dating

Three sets of samples were collected from sections within Silver Lake quarry (Figs. 3–6). Samples UCR120 to UCR126, SL-1 to SL-3, and UCR122 (dup) to UCR123 (dup) were analyzed at the Luminescence Dating Laboratory at the University of California, Riverside, the Physical Research Laboratory in Ahmadabad, and the USGS Luminescence Laboratory in Denver, respectively. Samples for optically stimulated luminescence (OSL) dating were collected by hammering light-tight metal and plastic tubes into freshly exposed sediments or by collecting large ($>30\times30\times30$ cm) blocks of sediment, which were wrapped in aluminum foil and stored in light-proof bags. The tubes and blocks remained sealed until processed under safe light conditions. Each sample was individually sampled and processed separately.

4.4.1. Samples UCR120 to UCR126 (measurements at Riverside)

The in situ water content (mass of moisture/dry mass; Aitken, 1998) was determined using sub-samples by drying them in an oven at 50 °C. The grain-size fraction 90–125 μm for dating was obtained by dry-sieving. The carbonates and organic matter were removed from the 90–125 μm fraction using 10% HCl and 30% H_2O_2, respectively. Sodium polytungstate solutions of different densities and a centrifuge were used to separate the quartz and feldspar-rich fractions. The separated quartz-rich fraction was treated with 49% HF for 80 min to dissolve any plagioclase feldspars and remove the α-irradiated surface of the quartz grains. Dried quartz grains were mounted on stainless steel disks using silicon spray. All the preparation techniques were carried out under laboratory safelights to avoid optical bleaching of the luminescence signal.

Approximately 20 g of the dried sub-sample from each sediment sample was ground to a fine powder and sent to the Becquerel Laboratories at Lucas Heights in Australia for instrumental neutron activation analysis (INAA). Using dose-rate conversion factors of Adamiec and Aitken (1998) and β attenuation factors of Mejdahl (1979) and Adamiec and Aitken (1998), the elemental concentrations were converted into external β and γ components, which were in turn corrected for moisture content. The cosmic ray dose was derived using Prescott and Hutton (1994) (Table 4).

The measured water content of the sediment was between ~1% and 2%. Enzel et al. (2003b) highlighted, however, that Silver Lake was filled for most of its duration during the Late Glacial–Early Holocene (~15–9 ka) and the spit would have likely been submerged. As such, the lake sediments most likely were saturated with water during much of the time that the lake existed. Given that the porosity of the sediment may be as high as 30%, assigning 10 ± 5% water content for the whole of the Late Glacial and Holocene provides us with a very liberal estimate and error range for water content that varies from 10 to 30%.

Luminescence measurements were undertaken using a Daybreak 1100 automated system with an 1100FO/L combined fiber-optic/IRLED illuminator for optical stimulation (Bortolot, 1997). Luminescence from the quartz grains was stimulated using a 150 W halogen lamp producing green light (514 ± 34 nm; ~20 mW cm^{-2}) defined by an additional narrow band interference filter. All quartz samples were screened for feldspar contamination using infrared stimulation from T-1 GaAlAs diodes (880 ± 80 nm). OSL signals were detected with a photomultiplier tube characterized by 9-mm Schott UG11 ultraviolet detection filters. Daybreak TLApplic 4.30 software was used for hardware control and equivalent dose (D_E) analysis.

D_E measurements were determined on multiple aliquots for each sample using the single aliquot regenerative (SAR) protocol developed by Murray and Wintle (2000). Each measurement cycle comprised a regeneration dose (zero for natural), preheating of 220 °C for 10 s, optical stimulation for 100 s at 125 °C, a test-dose, a cutheat of 160 °C and a final optical stimulation for 100 s (at 125 °C). The net-natural and net-regenerated OSL were derived by taking the initial OSL signal (0–1 s) and subtracting a background from the last part of the stimulation curve (90–100 s); subtracting the background from the preceding natural and regenerative OSL signals derived the net test-dose response. Growth curves were plotted using the net natural and regenerated data divided by the subsequent response to the net-test dose. The growth curve data was fitted with either a linear progression or single saturating exponential. The D_E for each sample was calculated using the mean values and standard error of all the aliquots for each sample (Table 4).

Probability plots were constructed to illustrate the spread of D_E values for each sample and support the use of a mean and standard error to calculate the OSL age for each sample (Fig. 10A). The INAA, cosmic dose rates, total doses, mean D_E and OSL ages are shown in Table 4.

Table 4
Data for optically stimulated luminescence and ages for samples collected at the Silver Lake quarry

Sample ID	LFA	K (%)[a]	Rb (ppm)[a]	Th (ppm)[a]	U (ppm)[a]	Water content (%)	Cosmic dose rate (Gy/ka)[b]	Total dose rate (Gy/ka)[c]	Number of aliquots[d]	Equivalent dose (Gy)[d,e]		Age (ka)[f]	
UCR122	4	2.09	83.8	8.25	0.81	2.0[g]	0.18±0.02	2.91±0.20	22/**19**	22.5±11.3/**22.7±11.9**		7.7±1.3/**7.8±1.1**	
UCR123	2	2.40	80.8	13.10	5.34	3.2[g]	0.19±0.02	4.57±0.28	36/**22**	19.9±8.0/**20.7±7.9**		4.4±0.5/**4.5±0.5**	
UCR124	4	1.97	77.5	13.40	10.6	1.4[g]	0.19±0.02	5.55±0.33	27/**13**	25.9±8.8/**28.8±8.8**		4.7±0.8/**5.2±0.5**	
UCR125	8	2.62	80.5	9.32	2.09	1.4[g]	0.18±0.02	3.81±0.26	20/**15**	24.8±5.8/**25.09±7.2**		6.5±0.7/**6.6±0.7**	
UCR126	6	2.21	90.7	9.85	3.33	1.1[g]	0.18±0.02	3.78±0.24	22/**9**	27.5±7.9/**24.7±4.0**		7.3±0.8/**6.5±0.6**	
SL-1	8	1.1±0.05	—	8.8±2.9	3.5±1.3	10±5	—	2.5±0.4	**64**	14.5±7.6		6±3	
SL-2	4	1.9±0.1	—	9.9±3.2	3.9±1.2	10±5	—	3.4±0.4	**53**	21±11.1		6±3	
SL-3	6	1.2±0.06	—	6.1±1.8	3.0±1.4	10±5	—	2.3±0.4	**68**	12.2±3.7		5±2	
										BLSL[h]	IRSL[i]	BLSL	IRSL
UCR122(dup.)	4	1.79	—	12.52	3.10	1[g]	0.19	3.68±0.15	Sample only measured to assess variation in dose rate				
UCR123(dup.)	2	2.43	—	13.02	2.95	1[g]	0.19	4.31±0.18	25/**21**	20.8±1.09		4.8±0.6	
UCR123(dup.)	2	2.43	—	13.02	2.95	1[g]	0.19	6.35±0.26			59.9±4.2		9.4±1.5

[a]Uncertainties on analyses of U, Th, Rb and K for UCR samples are taken to be ±10%.
[b]Cosmic doses and attenuation with depth were calculated using the methods of Prescott and Stephans (1982) and Prescott and Hutton (1994).
[c]For UCR samples the total doses combine the cosmic dose rate and the beta and gamma doses calculated from the K, Rb, Th and U concentrations in the sediment using the methods of Adamiec and Aitken (1998) and Mejdahl (1979) with corrections for moisture content after Zimmerman (1971).
[d]Total number of aliquots measured are shown in the normal text. The bold numbers indicate the number of aliquots used to calculate the D_E, which satisfy the recuperation and mismatch criteria.
[e]Average equivalent dose (D_E) and error ($1\sigma_{n-1}$ of the D_E), incorporating the error from beta source estimated at about ±5%.
[f]Ages calculated using all the aliquots measured are shown in the normal text. The bold numbers indicate the age based on the mean D_E, which satisfy the recuperation and mismatch criteria.
[g]Field moisture content, but 10±5% used in calculation of the dose rate.
[h]Blue light stimulated luminescence.
[i]Silt fraction (4–11 micron size) for IRSL as multiple aliquot additive dose technique (MAAD). *A*-value at 0.08 with errors on ages at 2 sigma.

The large spread of D_E suggests that the samples were partially bleached. The D_E values also include the analytical errors associated with measurement systems. By using the mean of the D_E distribution the OSL ages range from 4.5 to 7.8 ka.

4.4.2. Samples SL-1 to SL-3 (measurements at the Physical Research Laboratory)

Samples SL-1, SL-2 and SL-3 are coarse grained (90–125 μ). They were pretreated analogously to the UCR samples. A 5-point single aliquot regenerative (SAR) method was applied for D_E estimations. A preheat of 240 °C for 10 s was used to remove unstable signals for natural and regenerated doses. Blue light stimulated luminescence (BLSL) on all the samples was carried out in a Risoe TA-DA-12 reader. Detection optics was comprised of Schott BG-39 and U-340 filters. β-Irradiation was delivered using $^{90}Sr/^{90}Y$ source having a dose rate of 7.31 Gy min^{-1} for coarse-grained quartz. Examples of the distribution of D_E are shown in Fig. 10B. Such a

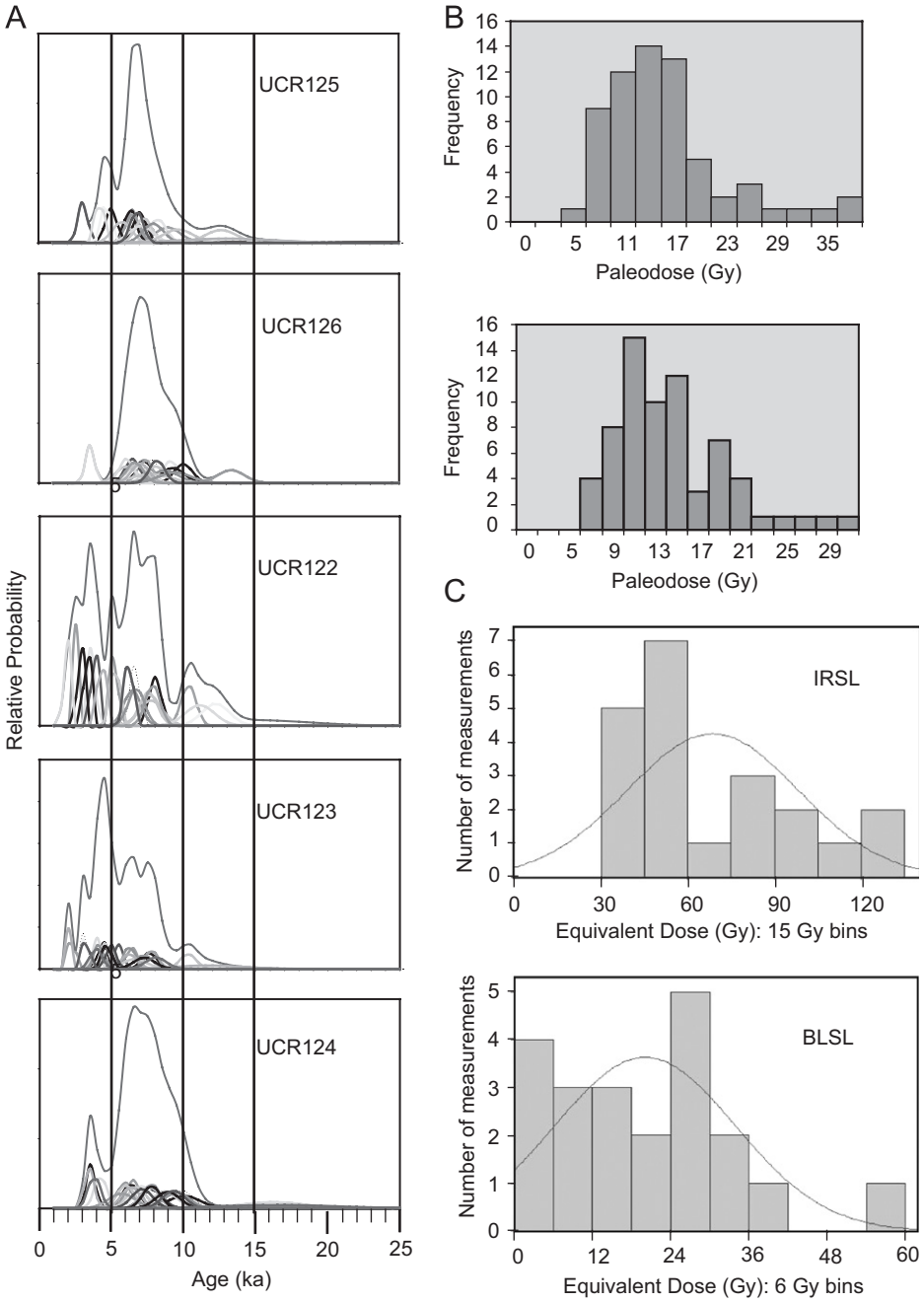

Fig. 10. Examples of the luminescence characteristics of the luminescence dating samples. (A) Probability plots of OSL dating samples dated at UCR; (B) examples of histograms of equivalent doses for selected samples processes at the PRL (upper and lower graphs are samples SL-1 and SL-2, respectively); and (C) examples of histograms of equivalent doses for selected samples processes at the USGS (upper and lower graphs are samples UCR123 (dup) and UCR122 (dup), respectively); (BLSL—blue light stimulated luminescence; IRSL—infrared stimulated luminescence).

distribution suggests partial bleaching. The results shown in Table 4 use both the mean of the distribution of D_E and the mean of the least 10% of the distribution. The latter assumes that the least 10% is representative of well bleached grains, while the other 90% of the distribution suffers from partial bleaching. The mean value is the average of the D_E obtained in this procedure. In this SAR procedure, natural sensitivity changes were monitored by introducing 110 °C TL measurement before and after making natural OSL measurement. The ratio of these two TL measurements was used to correct for any sensitivity changes that may have occurred (Jaiswal, 2005; Singhvi, 2007).

For dose rate calculations, uranium (U) and thorium (Th) concentrations were measured by thick source alpha counting (TSAC) using ZnS (Ag) screens on α counters-(583) from Daybreak. Potassium (K) concentrations were measured using NaI (Tl) γ spectrometry.

4.4.3. UCR122 (dup)–UCR123 (dup) (measurements at the USGS, Denver)

As a further test of the dose rates, another two samples (UCR122 (dup.) and UCR123 (dup.)) were obtained from near the location where UCR-122 and UCR123 were collected. The dose rates were determined from high-resolution γ spectrometry (Ge) and used Prescott and Hutton's (1994) calculations for the cosmic data. The dose rate data from this sample as well as the replicate sample UCR123 (dup) are shown in Table 4.

Sample preparation was only slightly modified from the techniques used in the UCR and Physical Research laboratories. Under safelights the carbonates and organic matter were removed from the bulk sample using 4 N HCl and 30% H_2O_2, then the sample was wet sieved to obtain the 90–125 μm fraction. Lithium sodium tungstate solutions of different densities and a centrifuge were used to separate the quartz and feldspar-rich fractions from the heavy minerals, while Stoke's settling was used to obtain the fine silt-sized fraction (4–11 μm) for infrared stimulated luminescence (IRSL) dating. The separated quartz-rich fraction was treated with 49% HF for 45 min to dissolve any plagioclase feldspars and remove the α-irradiated surface of the quartz grains. Dried quartz grains were mounted on stainless steel disks with silicon spray. For IRSL, polymineral silt was evaporated from a methanol slurry, covering the entire disk.

The sand-size samples of UCR123 (dup) was analyzed using SAR method (Murray and Wintle, 2000; Banerjee et al., 2001) with blue-light excitation. Dose recovery and preheat plateau tests were performed to ensure that the sediments were responsive to optical techniques and that the proper temperatures were used in producing the D_E values. Blue-light OSL measurements were made on a Riso TA-DA-15 TL/OSL reader, equipped with a β source for irradiations and blue LEDs (470 nm) providing approximately 15 mW cm^{-2} at 90% power. The blue-light OSL measurements were made at 125 °C after a preheat of 220 °C for 10 s with a cut heat of the same time and intensity and detected using three 3-mm Hoya U-340 filters. An IRSL stimulation of 100 s before the blue-light stimulation of 40 s was used to completely drain any residual feldspar contamination. UCR123 (dup.) provided a luminescence age of 4.8 ± 06 ka.

The fine-grain (4–11 μ) polymineral extracts from sample UCR123 (dup) was dated using the total bleach multiple aliquot additive dose (MAAD) method (Singhvi et al., 1982; Lang, 1994; Richardson et al., 1997; Forman and Pierson, 2002). IRSL measurements were accomplished using an automated Daybreak 1100 reader with infrared emissions (880 ± 80 nm; Spooner et al., 1990). The diode array delivers approximately 17 mW cm^{-2} and resultant blue emissions were measured at 30 °C after preheats of 140 °C for 7 h or 124 °C for 64 h. The IRSL detections were measured under a 3-mm Schott BG-39 and a Corning 7–59 glass filters that block >90% luminescence emitted below 390 nm and above 490 nm from the sediments. Blue-dominated emissions were chosen for the measurement because previous studies indicate greater suitability as a chronometer than ultraviolet wavelengths (e.g., Balescu and Lamothe, 1992; Balescu and Lamothe, 1994; Rendell et al., 1995; Lang and Wagner, 1996). IRSL ages on fine grained sediment are older (9.4 ± 1.5 ka) than the coarse grained quartz ages (Table 4). These are more in line with radiocarbon ages, and seem to obviate the need for an extensive correction factor (e.g., Huntley and Lamothe, 2001).

4.5. ESR dating

ESR dating of the *A. californiensis* shells collected from LFA 6 and LFA 8 was undertaken at the geochronology laboratories at the University of Koeln (Cologne). Details of the theory and methodology behind ESR dating of fossil mollusks is described in the pioneering research of Ikeya and Ohmura (1981) and Radtke et al. (1981). The substantial methodological progress made subsequently is summarized in Schellmann and Radtke (1999). An ESR age result is derived from the ratio of past natural radiation dose (D_E) to the annual dose rate (D'). It is crucial to determine the present and past D' when ESR dating mollusks. The D' of mollusks depends on the U content in the shell, and the U, Th, and K content in the matrix material and the cosmic dose rate. Problems ensue from the heterogeneity of the surrounding sediments and from the fact that both the sediments and the shells represent systems open to U migration. As shown by Schellmann and Radtke (1999), an early uptake model should be used for calculating the internal dose rate of the mollusk shells. The D_E value is determined by the additive dose technique which involves irradiating, usually with a strong gamma source, aliquots of the sample to increase trapped electrons within the minerals that constitute the shell, which in turn leads to an enhancement of the ESR signal. The ESR intensity versus the laboratory dose provides the dose

response curve that is used to fit to a saturating exponential. The extrapolation to zero intensity yields the D_E value on the intersection with the x-axis. The most suitable signal for dating aragonitic shells is $g = 2.0006$. The signal is radiation sensitive, and is stable over at least the last 300,000 years and gives realistic ages estimates. This contrasts with signals that have g-values of 2.0057, 2.0031, 2.0018 and 1.9973, which also increase with artificial radiation (for further details see Schellmann and Radtke, 1999, 2001).

All mollusk samples were etched by 0.1% HCl (up to 4×30 min) to remove the outer layers influenced by α-irradiation. After grinding and sieving, 20 aliquots of 0.1 g mass with 100–200 μm particle size were γ-irradiated with a ^{60}Co (Cobalt) γ source at the university hospital of Düsseldorf up to 30 Gy. The irradiation dose rate was 0.8 Gy min^{-1}. ESR intensities were measured using a Bruker ESP 300E spectrometer. Typical measurement parameters were 25 mW microwave power, 0.5 G modulation amplitude, 20.972 s sweep time, 40 G scan width, 1024 points resolution, and an accumulation of between 20 and 40 scans. D_E values were determined by using the program "fit-sim" of R. Grün (version 1993) and the "D-DP procedure" of Schellmann and Radtke (2001); and age calculations were carried out with the program "Data 7" of R. Grün (version 1999) using an α-efficiency (k-factor) of 0.1 ± 0.02.

The ESR ages range from 2.6 ± 0.3 to 4.7 ± 0.4 ka (Table 5). The high U concentrations in the shells ($U_{internal}$) suggest that the shells were open systems that allowed post-mortem enrichment of U. Therefore, the internal dose rate is problematic. Since ESR age calculation assumes an early U uptake, the ESR ages are questionable. The open U system means that the ESR ages are likely to be considerably younger than the true age of the shells and should therefore be considered as minimum ages. The application of ESR dating to *A. californiensis* shells at this site is therefore challenging. Unfortunately, as shown Kaufman et al. (1971), open U–Th systems are common in mollusks making the application of ESR methods to other genus besides *A. californiensis* also difficult.

4.6. AAR

Carbonate shells of ostracodes, peleycpods, and gastropods from three richly fossiliferous horizons in Silver Lake quarry were analyzed for the extent of AAR. The total hydrolyzable amino acid (THAA) fraction was analyzed from eight monospecific samples. Each ostracode sample was made up of seven individual valves, and each mollusk sample comprised five. Each shell was prepared and analyzed separately (46 total subsamples). In addition, we analyzed three samples of ostracodes for the extent of racemization in the naturally free amino acid (FAA) fraction. For the FAA, we used three valves per subsample because the amino acid concentrations were lower.

Samples were prepared and analyzed at the Amino Acid Geochronology Laboratory of Northern Arizona University according to methods by Kaufman and Manley (1998) with modifications for ostracodes described by Kaufman (2000). Briefly, the analytical method employed pre-column derivatization with *o*-phthaldialdehyde (OPA) together with the chiral thiol, *N*-isobutyryl-L-cysteine (IBLC), to yield fluorescent diastereomeric derivatives of chiral primary amino acids. The derivatization was performed on-line prior to each injection using an auto-injector. Separation was by a reverse phase column packed with a C_{18} stationary phase (Hypersil BDS, 5 μm) using a linear gradient of aqueous sodium acetate, methanol and acetonitrile. Detection was by fluorescence. Hydrolysis was achieved using 6 M HCl, sealing under N_2, and heating at 110 °C for 6 h. The hydrolysates were then evaporated to dryness in vacuum and rehydrated in 10 mM HCl before injection into an integrated Agilent HP1100 liquid chromatograph. Each subsample was injected once. The average analytical uncertainty (internal reproducibility) measured by the coefficient of variation ($CV = \bar{\chi}/\sigma$) for multiple injections of laboratory standards is typically between 3% and 5% for most of the amino acids. For this study, we focus on aspartic acid (Asp) and glutamic acid (Glu), two amino acids that are among the most abundant enantiomers, are the best resolved chromatographically, elute during the first 30 min of the sample run, and span

Table 5
Electron spin resonance dating results

Sample laboratory number	LFA	K_{ext} (%)[a]	$Th_{external}$ (ppm)[a]	$U_{external}$ (ppm)[a]	$U_{internal}$ (ppm)[a]	Water content (%)	Depth (m)	Total dose rate (Gy/ka)[b]	D_E (Gy)[c]	Age (ka)[d]
K-5300	6	1.30	15.06	7.37	9.72	3±2	0.7	3.68±0.13	17.20±1.36	4.7±0.4
K-5001	6	1.30	15.06	7.37	13.11	3±2	0.7	3.85±0.17	16.79±1.14	4.4±0.4
K-5002	6	1.30	15.06	7.37	12.04	3±2	0.7	3.68±0.13	15.44±1.10	4.1±0.3
K-5303	8	1.25	20.60	14.76	2.21	3±2	0.6	3.66±0.06	9.38±0.96	2.6±0.3

[a]Uncertainties on ICP-MS analyses of U, Th and K are taken to be ±1%.

[b]For *K* samples the total doses combine the cosmic dose rate (see b in Table 4) and the β and γ doses from the K, Th and U concentrations in the sediment and the α, β and γ doses from the U concentrations in the shells. Sample thickness was 1.1–1.7 mm, removed thickness was 0.3–0.6 mm (age calculation with β-attenuation).

[c]D_E = Equivalent dose (Calculated via program FIT-SIM (R. Grün).

[d]Ages calculated via program DATA 7 (R. Grün).

Table 6
Extent of amino acid racemization (D/L) in ostracodes and mollusks from Silver Lake Quarry

Lab ID (UAL)[a]	Taxon	Asp D/L		Glu D/L		n[b]	ex[b]
		Ave	$\pm\sigma$	Ave	$\pm\sigma$		
Unit LFA4/unit b (~15.5 ka); depth = 160 cm							
4168	Anodonta	0.714	0.022	0.506	0.030	7	—
4167	*Gyralus*	0.704	0.035	0.527	0.042	5	—
4146	*Limnocythere ceriotuberosa*	0.480	0.018	0.355	0.007	5	—
4146F	*Limnocythere ceriotuberosa*	0.774	0.007	0.525	0.033	7	—
Unit LFA6/unit d (12.5 ka); depth = 90 cm							
4169	*Anodonta*	0.790	0.019	0.649	0.044	6	1
4145	*Limnocythere ceriotuberosa*	0.549	0.014	0.424	0.013	5	—
4145F	*Limnocythere ceriotuberosa*	0.744	0.035	0.555	0.015	6	1
Unit LFA8/unit f (~11.8 ka); depth = 70 cm							
4171	*Anodonta*	0.762	0.019	0.617	0.017	7	—
4170	*Physa*	0.704	0.038	0.516	0.045	4	1
4147	*Limnocythere ceriotuberosa*	0.534	0.012	0.433	0.008	5	—
4147F	*Limnocythere ceriotuberosa*	0.782	0.012	0.587	0.012	6	1

[a] F = Free amino acid fraction; others are total hydrolyzable amino acids.
[b] n = Number of subsamples used to calculate the average and standard deviation; ex = number of subsamples rejected.

most of the range of racemization rates. More accurately, the Asp and Glu may include a small component of asparagine and glutamine, respectively, which were converted to Asp and Glu during laboratory hydrolysis.

Of the 67 analyses, three were rejected because they exhibited high concentrations of the labile amino acid serine (L-Glu/L-Ser values < 1.0; Kaufman, 2000), indicative of modern contamination, and one was rejected because its D/L values fell beyond $\pm 2\sigma$ of the mean of the others. In all, four subsamples (6%) were excluded (Table 6). D/L values are reported as the mean $\pm 1\sigma$ of the multiple subsamples. D/L values in gastropods showed higher variability than for ostracodes or pelecypods. The average CV for the 11 samples was 3% for Asp D/L and 5% for Glu D/L, which is well within the range expected for a single-age population of shells. The results from the different taxa are mutually consistent (Fig. 11). The multiple analyses on ostracodes, gastropods, and pelecypods all show that shells from the lowest and oldest of the three units (LFA4/unit b) have the lowest D/L. The higher D/L values in the younger samples highlight the control of burial depth and thermal histories on the rate of racemization. As expected, the extent of racemization in the FAA is higher than in the THAA.

Interpreting the extent of AAR in terms of sample age requires an equation that relates D/L to age for a given taxon and amino acid. Most importantly, the rate of racemization needs to be calibrated locally because the reaction rate is strongly dependent on ambient temperature. Presently, no age equations are available for AAR in shells of any type from the Mojave region. Nearly all previous amino acid geochronology in hot desert settings has been based on the amino acid isoleucine and cannot be

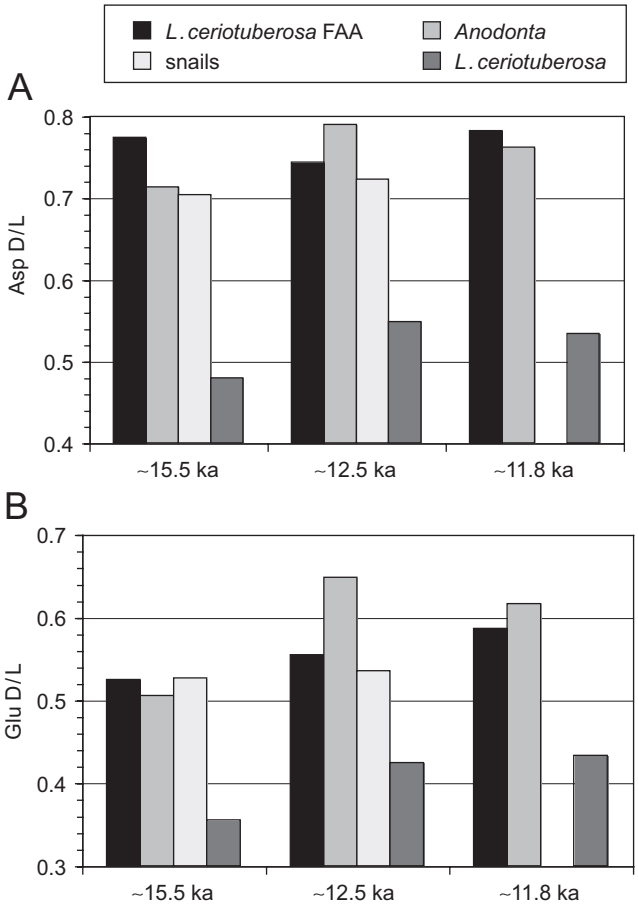

Fig. 11. Extent of amino acid racemization for (A) aspartic acid (Asp), and (B) glutamic acid in ostracodes (*Limnocythere ceriotuberosa*), snails (*Physa* and *Gyralus*) and plycepods (*Anodonta californiensis*) from three samples at Silver Lake quarry. Data listed in Table 6.

directly applied to our results. Therefore, instead of using the amino acid data to infer sample age, we assume that the ages for the samples are correctly represented by their ^{14}C ages (this study and Ore and Warren, 1971), and we use a previously determined relation between D/L, time, and temperature (Kaufman, 2000) to determine whether the assumed ages yield reasonable paleotemperature estimates.

To interpret D/L in terms of paleotemperature, the kinetics of the racemization reaction, including the temperature sensitivity of the forward rate constant, must be known. The paleotemperatures calculated in this study are based on an investigation of racemization kinetics in ostracodes (Kaufman, 2000), which included an analysis of both fossil and laboratory-heated shells. Laboratory heating experiments were used to evaluate the reaction rates of amino acids in ostracodes over a range of temperatures (80–140 °C) and D/L values (~0.1–0.6 in Asp). In addition to data from the heating experiments, the evaluation of racemization kinetics was extended to ambient temperatures using unheated, fossil ostracode shells from six ^{14}C-dated sites in the Bonneville basin, Utah. These data were used together to calculate the Arrhenius parameters (activation energy and frequency factor) for racemization in the ostracode genus *Candona*. All of the analyses on ostracodes from Silver Lake are on *Limnocythere*. The two ostracode genera appear to racemize at approximately the same rate (Kaufman, 2003), although the paucity of analyses does not allow confirmation of this observation.

Temperature, calculated based on amino acid paleothermometry, is the effective diagenetic temperatures (T_{eff}; Wehmiller, 1977). It is the weighted average post-depositional temperature that integrates the thermal history of a shell. Because the rate of racemization is dependent exponentially on temperature, the T_{eff} of a fossil will be weighted toward the higher temperatures that it experienced, and will be somewhat higher than the arithmetic mean annual temperature (T_{ma}). The extent to which it is higher is proportional to the amplitude of the postdepositional temperature variation (Miller and Brigham-Grette, 1989), and to the difference between ground temperature and air temperature (Wehmiller et al., 2000). For this reason, sample depth is a key variable at high-temperataure sites. By integrating the entire postdepositional temperature history of a deposit, the amino acid data provide a means of evaluating long-term temperature changes *since* the time that a deposit formed, rather than *during* deposition.

The relation between time, D/L and T_{eff} derived for *Candona* is (Kaufman, 2000)

$$T = -E_a/R\ln([(1 + D/L)/(1 - D/L)]^n - C/2At), \quad (2)$$

where A is the frequency factor (yr^{-1}); E_a the activation energy ($kcal\,mol^{-1}$), R the gas constant (0.001987 kcal $K^{-1}\,mol^{-1}$); $T = T_{eff}$ (K); $n = 3.6$ for Asp and 3.8 for Glu; and C is the power-law-transformed D/L measured in modern shells following laboratory hydrolysis (= 0.041 for Asp and 0.017 for Glu).

Assuming that Eq. (2) also applies to *Limnocythere*, and that the ^{14}C ages at Silver Lake quarry are correct, then the T_{eff} required to explain the D/L values can be evaluated (Table 7). The D/L values from the lowest and oldest unit, LFA4/unit b (~15.3–15.9 ka), suggest an T_{eff} of 19 °C for Asp and 25 °C for Glu. The D/L values from the younger units LFA6/unit d and LFA8/unit f (~11.8–12.5 ka) suggest an T_{eff} of about 26 °C based on Asp, and about 32 °C for Glu, or about 7 °C higher than for the older LFA4/unit b. Theoretically, the T_{eff} calculated for the two amino acids should overlap within errors. The error was estimated to be about ±2 °C for *Candona* from the Bonneville basin (Kaufman, 2003). The cause of the difference in T_{eff} inferred from the two amino acids is unknown, but might be related to the taxonomic effect, or to the fact that the equations were developed using samples with D/L values that were generally lower than those measured at Silver Lake.

Nonetheless, the modern ground temperature data from the region may be examined to assess whether the calcuated T_{eff} are resonable, or whether these data suggest either a younger or older age for the samples. The closest long-term weather station is Daggett, California, where the T_{ma} for the period of 1948–2005 was 20 °C (www.wrcc.dri.edu). The T_{ma} is necessarily lower than the T_{eff} because the

Table 7
Effective temperatures calcuated based on racemization in shells and for each sample depth based on instrumental data

Unit	Depth (cm)	Age (ka)	Racemization T_{eff} (°C)[a]		Current ground temp (°C)[b]	ΔT (°C)[c]	T_{eff} (°C)[d]
			Asp	Glu			
LFA8/unit f	70	~11.8	25	32	16	6	27
LFA6/unit d	90	~12.5	26	31	14	5	26
LFA4/unit b	160	~15.5	19	25	9	2	23

[a]Calculated based on Eq. (2) and D/L ratios listed in Table 4.
[b]Based on mean annual temperature (T_{ma}) = 21.0 °C at the suface and temperature attenuation measured in Imperial Valley, California (Fig. 11).
[c]Increase in effective temperature resulting from summer heating according to the equation (Miller and Brigham-Grette, 1989): $\Delta T = 0.039(T_{amp})^{1.813}$, where T_{amp} = amplitude of the annual temperature wave (Fig. 11).
[d]Estimated effective temperature = $T_{ma} + T_{amp}$, where T_{ma} = 21.0 °C.

amplitude of the annual temperature cycle is greater at shallower depth. Greater amplitude results in a greater effect on the T_{eff}. To assess the amount that the T_{ma} underestimates the T_{eff}, we examined the ground temperature profiles from Imperial Valley, California measured during 1964–1970 (Hu and Feng, 2003) (Fig. 12). These are the longest-term ground-temperature records that we know of from the region. They show the expected exponential attenutation in the amplitude of the annual temperature wave: from about 6 °C at 70 cm to 2 °C at 160 cm. Based on the relation between the amplitude of the temperature cycle and the corresponding shift in T_{eff} developed by Miller and Brigham-Grette (1989), the current T_{eff} at 70–90 cm depth is about 3–4 °C higher than at 160 cm. Taking this effect into account results in current T_{eff} estimates ranging between 23 and 27 °C for the sample depths.

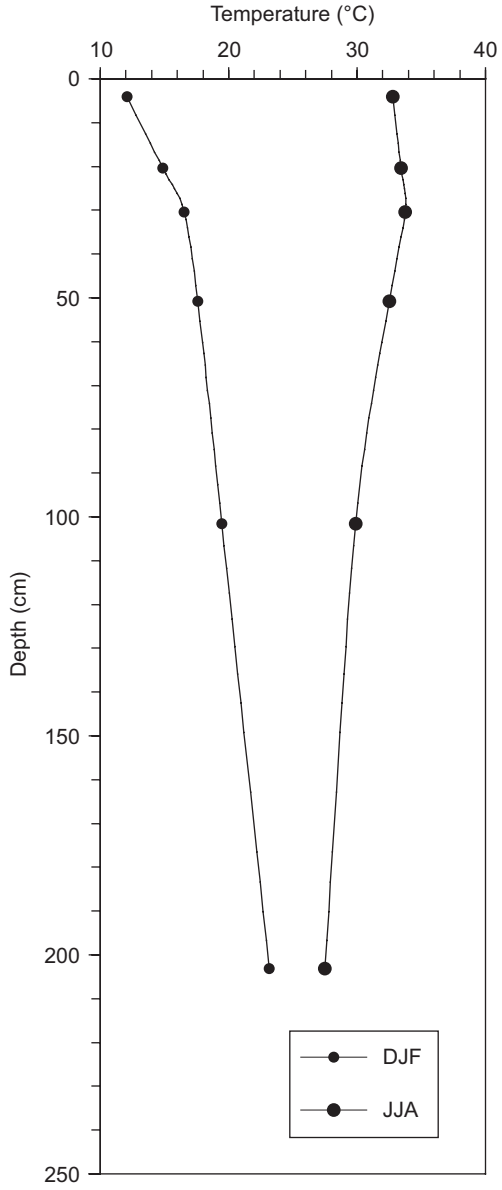

Fig. 12. Average winter (DJF) and summer (JJA) temperature measured below the ground surface between 1964 and 1970 at Brawley, Imperial County, California (Hu and Feng, 2003). The attenuation of the annual temperature wave was used to estimate the effective temperature at the depth of samples collected from Silver Lake quarry.

The current T_{eff} for the lower sample (LFA4/unit b) (23 °C) is bracketed by the T_{eff} estimates based on the racemization of Asp and Glu. Therefore the age assigned to the this sample (~15.3–15.9 ka) is consistant with the extent of racemization and the equations of Kaufman (2000). Whether the T_{eff} estimated based on Asp (19 °C) or Glu (25 °C) is more reasonable depends on assumptions about the thermal history of the sample. The lower temperature is more reasonable if the postdepositional history includes a signficant interval of submergance by lake water, which seems likely. Subaqueous temperature (especially summer temperature) is probably much lower than subaerial temperature. On the other hand, if the sample experienced relatively high temperatures during the middle Holocene, then the current T_{eff} of the site may be underestimated.

The current T_{eff} estimated for the upper samples overlap with those based on Asp D/L, but are lower than calculated for Glu D/L. The T_{eff} calculated based on Glu D/L are unexpectedly high, even when taking into account the effect of summer heating at shallow depth. To lower the calculated T_{eff} would require increasing the assumed ages for these samples, which seems unlikely when considering the luminescence data and any possible effect of hardwater that might bias the ^{14}C ages. Conversely, to satisfy both the luminescence ages and Eq. (2) would require T_{eff} that are 5 °C higher than those reported above, that is, 25° for Asp and 30 °C for Glu in the lowest sample. Although Glu D/L indicates a higher T_{eff}, the difference between the T_{eff} calculated for the lower and upper samples is the same for both Asp and Glu (6–7 °C). This is about twice the difference based only on the effect of the attenuation of the current annual temperature wave. The additional difference could be explained if the lower unit (2.5–3.5 m above the present playa floor) experienced an interval of inundation that the younger samples did not. For example, if the older unit was inundated for 5000 yr under 5 °C water, then the overall T_{eff} for the integrated ~15 ka history would decrease by about 3 °C. In other words, the younger samples experienced higher temperatures both because they are buried at more shallow depths (3 °C effect), and because they experienced a smaller proportion of their postdepositional history under a Late Quaternary lake (an additional 3 °C effect).

In summary, the D/L ratios in ostracodes, gastropods, and pelecypods from three units in the Silver Lake quarry are consistent among taxa, and for the FAA and THAA fractions. The Asp D/L values in ostracodes are also consistant with existing equations that relate D/L to sample age and postdepositional temperature. Assuming that the ^{14}C ages of the stratigraphic units are correct (Section 4), the D/L-Asp values suggest an T_{eff} of about 19 °C for the 15.3–15.9 ka shells (LFA4/unit b) and about 25 °C for the 12.5–11.8 ka shells (LFA6 and LFA8/units d

and f). If the OSL ages of 6–7 ka are correct then the estimates will be about 5 °C higher.

These values are in agreement with modern air and ground temperature data, and the higher D/L measured in the younger samples can be explained by the attenuation of the annual temperature wave with depth, and the likelihood that the older samples experienced an interval of lower temperature under Holocene lake water. The interconsistancy of the results therefore suggest that the radiocarbon ages are more accurate than the OSL ages.

4.7. U-series trial analyses

Two samples of Silver Lake tufa-coated shoreline gravel were analyzed for U–Th isotopes to assess the feasibility of obtaining reliable U-series ages for paleo-shorelines of Silver Lake (Table 8). The analyses were by thermal ionization mass spectrometry using methods similar to those of Sharp et al. (2003). Samples were completely dissolved using hydrofluoric and nitric acids in order to obviate possible fractionation of U/Th ratios and uranium isotopes that may result from partial dissolution of impure carbonates (e.g., Bischoff and Fitzpatrick, 1991).

The tufa samples contain ~1.3–2.3 ppm ^{232}Th, much higher than expected for pure, authigenic carbonate (in light of the very low solubility of Th in most natural waters). The source of this Th is probably included clays, or possibly, in part, "hydrogenous Th", that is, greatly elevated levels of Th dissolved in alkaline, saline lake waters as a result of complexation with CO_3^{2-} (for example, Anderson et al., 1982; Lin et al., 1996). Thus, significant initial ^{230}Th may have been present and must be subtracted in order to calculate meaningful ages. Thorium-232 may be used as an index isotope if the ^{230}Th/^{232}Th ratio of initial Th is known. The (^{230}Th/^{232}Th) activity ratios expected for clays (say, 0.6–1.0) and alkaline lake waters (up to ~1.9, Anderson et al., 1982), nearly encompass the observed (^{230}Th/^{232}Th) activity ratios of the Silver Lake tufas (~1.5–2.4). Accordingly, meaningful ages cannot be obtained by single-sample, total-dissolution U-series analyses. If coeval samples with sufficient spread in ^{238}U/^{232}Th ratios can be found, an isochron approach could yield improved U-series tufa ages. Even isochrons may not entirely obviate the effects of hydrogenous Th, however, if initial ^{230}Th is directly incorporated into carbonate, causing initial ^{230}Th to correlate positively with carbonate ^{238}U/^{232}Th ratios (Lin et al., 1996).

5. Discussion

The spit-shoreline complex in our study provides an unusually well-exposed and preserved example of shoreline landforms and strata that are common in Late Quaternary lake basins of the Great Basin, including Lake Lahontan, Nevada (e.g. Adams and Wesnousky, 1998). The shorelines east of the spit have small ($<100\,m^2$) wave-cut areas of bedrock and numerous bouldery and cobbly surfaces (Figs. 1 and 2). The sediments that comprise the spit are dominated by pebble and cobble clasts derived from the east by littoral drift. These sediments form decimeter- and meter-thick beds that were deposited as broad inclined beds mimicking an open fold (Fig. 4), probably during storms. The spit sediments fine to the west and north into sandy silt representing highwater stands and slackwater deposits behind the spit containing life assemblages of *A. californiensis*, gastropods and ostracodes (Figs. 2–6). The elevations of the highest and lowest shorelines (defined by differential GPS) are shown in Fig. 2. These heights were likely controlled by progressive incision of the spillway channel at the northern end of Silver Lake described by Ore and Warren (1971).

Our geochronological results suggest an intricate history for the spit-shoreline complex (Fig. 13). The TCN ages imply that the shorelines probably started to form sometime between 20 and 30 ka. However, the spread of ages for each of the shorelines suggest a complex pattern of inheritance of TCNs and exposure history (possibly including erosion of an irregular surface and toppling of boulders). Furthermore, the site was probably prone to successive periods of shielding by water during high stands or by sediments that were subsequently eroded. A TCN age of 20–25 ka for the initial shorelines is consistent with the age estimates for Lake Mojave I based on sedimentation rates determined by radiocarbon dating of cores from Silver Lake (Brown and Rosen, 1995; Enzel et al., 2002; Wells et al., 2003). Given the wide range of TCN ages, it is not possible to attribute a particular shoreline at this location to a time of high lake level. Since our work was completed, additional investigations in an arroyo north of Bench Mark Bay and between Bench Mark Bay and the Lake Mojave outlet channel has produced tufa radiocarbon ages of 16.1–17.6, and 14.8–17.1 and $\gg$25 ka on two higher and earlier lake stands, respectively (Warren and Ore, 2004a, b); these are consistent with the radiocarbon ages from sediment cores by Wells et al. (2003).

Table 8
U-series data

Sample ID	Sample wt. (mg)	U (ppm)	(^{234}U/^{238}U)act.	^{232}Th (ppm)	(^{232}Th/^{238}U)act.	(^{230}Th/^{232}Th)act.
SLQ W1	80.82	7.02	1.3066±0.0017	2.32	0.1091±0.0013	2.390±0.031
SLQ W2	171.41	3.54	1.2822±0.0018	1.26	0.1175±0.0094	1.537±0.12

Note. Errors are 95% confidence intervals. Isotope ratios are activity ratios.

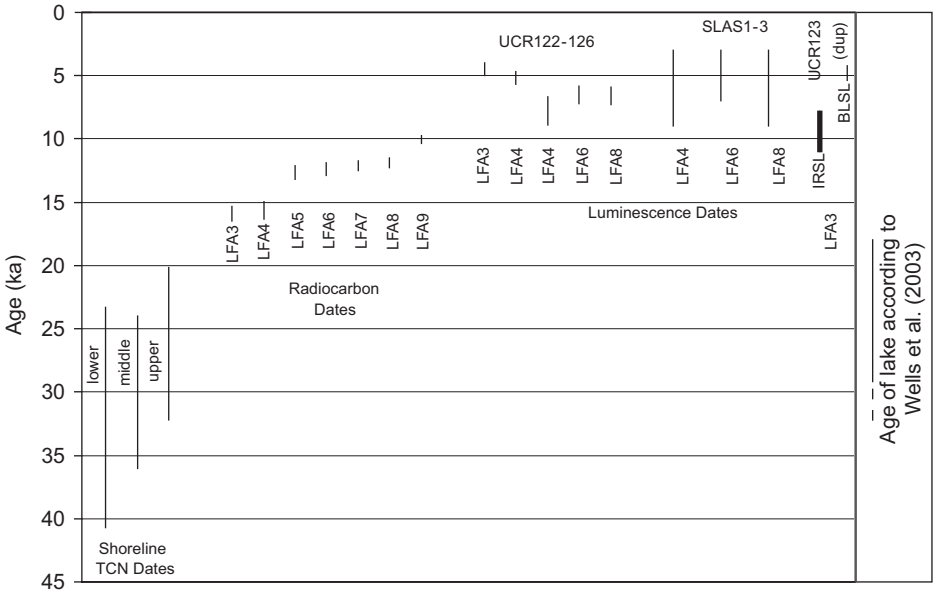

Fig. 13. Comparison of the range of ages obtained from the Silver Lake spit-shoreline complex using different methods. The TCN age ranges are shown as the 1 standard deviation about the mean for all the data for each shoreline. The radiocarbon age ranges are shown as three standard deviations about the mean for the combined radiocarbon ages for each lithofacies association (LFA). The luminescence age ranges are shown as 1 standard deviation about the mean.

Radiocarbon dating of tufa and *A. californiensis* from the gravel quarry exposure within the spit suggests that the spit began to form prior to 16 ka, and that it continued to build episodically until about 10 ka. The stratigraphic consistency and younging upward of the radiocarbon ages, for both the conventional ages of Ore and Warren (1971) and the new AMS ages, provide confidence in the radiocarbon ages for these deposits. Furthermore, the preservation of articulated *A. californiensis* shells in at least 3 units and life assemblages of ostracode valves in two of the fine-grain sediments interbedded between the tufa-covered gravels, suggest that the shells have not been transported a significant distance. The spit and the associated slackwater deposits record a history of alternating lake levels during Late Pleistocene and Early Holocene times. Wells et al. (2003) also reached this same conclusion.

In contrast to the radiocarbon, the luminescence dating of sediments within the spit suggest that they were deposited relatively rapidly during the early part of the mid Holocene (6–7 ka). The OSL dating was tested by replicating the analyses in three laboratories on subsamples from selected LFAs. The replicates have similar ages; however, they vary within a few hundred years among the laboratories. We attribute these interlaboratory differences to the different calculation methods. The data provide confidence that the discrepancy between OSL and radiocrabon are not the result of OSL laboratory error. However, some of the luminescence ages are not stratigraphically consistent; for example, samples UCR123 and 124 have younger ages than the samples for overlying beds. These reversals in ages are attributed to the anomalously high dose rates for these two samples compared to the other samples. The high dose rates might be due to detrital ^{230}Th, which would have been counted as ^{238}Th in the dose rate determination (Table 4). This could also be an artifact of some carbonate contamination that lead to local scale dosimetric changes.

Nevertheless, all the OSL ages (6–7 ka) suggest a much younger age for the deposits than the radiocarbon dating (15–9 ka). The young OSL ages are unexpected as possible partial bleaching prior to deposition should lead to an overestimate of the age. OSL ages can be underestimated by thermal fading, especially for volcanic feldspar. However, the geologic maps of immediate local region show that the it is devoid of volcanic rocks that could provide volcanic feldspar, and our one IRSL analysis of feldspar, with an age of 9.4 ± 1.5 ka, contrasts with quartz OSL. A third possibility for the young ages is the infiltration of younger sand grains through desiccation cracks. This seems unlikely given the compact nature of the silty sand layers. We have assumed water content of 10% for the age calculations, although the samples were nearly dry when collected. If the average water content was 20% then the luminescence ages are likely to be underestimated by 10–15%, which is still much younger than the radiocarbon results. Higher water contents would almost proportionately increase the age.

Another possibility to explain the OSL-radiocarbon disagreement is that the radiocarbon ages may be systematic overestimates. Numerous studies indicate that radiocarbon ages on carbonate shells may be overestimated on account of hardwater effect (e.g., Juyal et al., 2004),

especially in areas that contain carbonate rocks. Carbonate bedrock is present but sparse in the Mojave River drainage and might contribute to a hardwater effect. Carbonate dust, however, might contribute substantially to the lakes in the Mojave. The new ages on paired samples of charcoal and shell from Cronese basin, however, indicate no significant hardwater effect, although the Cronese and Silver lake basins have the same surface water sources the results may not be directly applicable to the Silver Lake spit because the local geology is different as well as potential sources of groundwater. Berger and Meek (1992) found a relatively minor (450 year) hardwater effect for *A. californiensis* in the area. Furthermore, AAR on ostracode valves supports the Late Glacial or Last Glacial Maximum age for the formation of the spit because, when applied to the age equation of Kaufman (2000), the radiocarbon ages suggest post-depositional temperatures that agree with the available data. For the spit to be younger than the radiocarbon age would imply untenably high post-depositional temperatures. Moreover, the sedimentology and radiocarbon ages are consistent with the current understanding of the regional paleoenvironmental changes during the Late Glacial and Holocene timing of lakes found in the sediment and soil development of the deposits (see papers in Enzel et al., 2003a). This supports the interpretation that the radiocarbon dating of the spit and shoreline is accurate and consistent.

In an attempt to resolve the difference between the radiocarbon and OSL ages, we applied ESR dating to *A. californiensis* shells from selected sediment and U-series dating on tufa from within the spit. Unfortunately, the ESR dating was unsuccessful. This is not surprising because most mollusc shells (such as *A. californiensis*) behaved as open systems allowing post-mortem enrichment of U and hampering dose-rate determination. As such the ESR ages can only be considered as minimum-limiting ages. These results stress the need to be cautious when applying ESR methods to these and similar deposits.

The U-series failed as well because of the presence of substantial ^{232}Th, probably indicating the presence of contaminating silicate detritus in the form of clays. These observations support why the OSL ages. However, this might be overcome by collecting and analyzing coeval samples of tufa to provide a sufficient spread in ^{232}Th/^{238}U ratios so that an isochron approach could yield improved U-series tufa ages.

The focus of future work which would include:

1. Elucidation of any radiocarbon reservoir age for these samples by comparing charcoal with shells, such as *A. californiensis*.
2. Elucidation of the causes of OSL ages being younger by examining the micromorphology of sediments and evidence of any contamination.
3. Independent estimation of paleotemperatures during the Holocene using stable isotopes.
4. Understanding of the causes of difference in paleotemperature estimates based on amino acid results.

Given that each of the geochronology methods record the rate of physical and chemical processes, there is need to understand the underlying effects. The concordance or discordances between methods and methodologies have to be explained on sound physical and chemical reasoning and field geomorphology. This study elucidates the needs for multiproxy dating from any such terrestrial site. However, in reality, it is difficult to successfully apply multiple dating techniques to most terrestrial sites, since each method has its own inherit problems that may be site or sample dependent. Furthermore, it is extremely difficult to find appropriate sites where numerous geochronological techniques can be applied and cross-checked, especially when the dating methods are applied to landforms that are not necessarily contemporaneous (e.g., the spit and shorelines analyzed in this study).

6. Conclusions

The results presented in this study provide insights into the evolution of a Late Quaternary spit-shoreline complex at the north end of Silver Lake playa, and they illustrate the benefits and difficulties of applying multiple numerical dating techniques. The TCN ages suggest that the erosional shorelines probably began to develop ~25 ka. The influence of inheritance of TCNs during prior exposure is difficult to deduce, however, because the amount of rock was removed to form the shorelines is not accurately known. This uncertainty is likely to decrease TCN ages by a few thousand years. A shoreline age of between 20 and 25 ka is consistent with the estimates determined by sedimentological studies in Soda and Silver Lakes (Brown and Rosen, 1995; Wells et al., 2003).

Our new AMS radiocarbon ages are consistent with the conventional radiocarbon ages of Ore and Warren (1971), which suggest that the spit and lagoonal/backwater sediments were deposited during Late Glacial to Early Holocene during times of rapid lake-level fluctuations. This significantly post-dates the initial formation of the bedrock shorelines. Applying Bayesian analysis to the radiocarbonages provides high precision for each of the sedimentary units that were dated. Uncertainties related to hardwater effects in Silver Lake have not been resolved, but a comparison of radiocarbon dates on *A. californiensis* shells and charcoal in the adjacent Cronese Lake basin suggests that hardwater effects was probably small. The AAR data support the radiocarbon ages for spit formation during the Late Glacial.

In contrast, the OSL ages on sediments in the spit suggest early-Mid Holocene ages. The OSL ages at this site are likely incorrect, given the systematic reproducibility of radiocarbon chronologies throughout the Great Basin. We cannot explain the difference between the luminescence and radiocarbon ages, and clearly such differences need to be

the focus of future work. We caution researchers in desert environments to be aware of the problems associated with both radiocarbon and OSL dating when interpreting the ages of landforms based on only one of these methods. Nevertheless, there are numerous good example of where luminescence and radiocarbon dating works well in desert environments (e.g., Forman and Pierson, 2002).

ESR dating of *A. californiensis* shells was problematic due to the post-mortem enrichment of U in their shells. This made dose-rate determination problematic and as such the ESR ages can only be considered as minimum estimates. We therefore stress the need to be cautious when applying ESR methods to these and similar deposits.

High concentrations of detrital Th within tufa inhibited the use of U-series to date the tufa. However, U-series tufa ages might be determined by collecting and analyzing coeval samples of tufa to provide a sufficient spread in $^{232}Th/^{238}U$ ratios so that an isochron approach could be applied. We recommend such as the approach for future work.

The present study outlines the need for concentrated research at key sites, such as this, to help refine methods, understand their problems and applicability and develop new ways of utilizing numerical dating techniques, conjunctively. Furthermore, the use of multiple dating techniques promises to provide more details on chemical and physical processes within arid and semi-arid environments. Each of the methods provides information that relates to both geochronology as well as some aspect of the physical/geochemical processes that may have affected the samples.

Acknowledgments

Thanks to Jeffrey Knott, David Miller and Yehouda Enzel for their constructive and extremely useful reviews of our manuscript. The original fieldwork was funded by the Western Center for Archaeology and Paleontology, California. The amino acid analyses were funded by a cooperative agreement with the USGS, Earth Surface Dynamics, and by an NSF Facilities Support Grant EAR-0419617. This research was performed under the auspices of the US Department of Energy by the University of California, Lawrence Livermore National Laboratory under Contract No. W-7405-Eng-48. AKS thanks UC Riverside for support for the field visit and the University of Heidelberg for support and facilities during the manuscript preparation. MJ thanks the Director of the Wadia Institute for Himalayan Geology for support.

References

Adamiec, G., Aitken, M., 1998. Dose-rate conversion factors: update. Ancient TL 16, 37–50.

Adams, K.D., Wesnousky, S.G., 1998. Shoreline processes and the age of the Lake Lahontan highstand in the Jessup embayment, Nevada. Geological Society of America 110, 1318–1332.

Aitken, M.J., 1998. An Introduction to Optical Dating. Oxford University Press, Oxford.

Anderson, R.F., Bacon, M.P., Brewer, P.G., 1982. Elevated concentrations of actinides in Mono Lake. Science 216, 514–516.

Balescu, S., Lamothe, M., 1992. The blue emission of K-Feldspar coarse grains and its potential for overcoming TL age underestimation. Quaternary Science Reviews 11, 45–51.

Balescu, S., Lamothe, M., 1994. Comparison of TL and IRSL age estimates of feldspar coarse grains from waterlain sediments. Quaternary Science Reviews 13, 437–444.

Banerjee, D., Murray, A.S., Botter-Jensen, L., Lang, A., 2001. Equivalent dose estimation using a single aliquot of polymineral fine grains. Radiation Measurements 33, 73–94.

Berger, R., Meek, N., 1992. Radiocarbon dating of *Anodonta* in the Mojave Basin. Radiocarbon 34, 578–584.

Bischoff, J.L., Fitzpatrick, J.A., 1991. U-series dating of impure carbonates: an isochron technique using total-sample dissolution. Geochimica et Cosmochimica Acta 55, 543–554.

Bortolot, V.J., 1997. Improved OSL excitation with fiber optics and focused lamps. Radiation Measurements 27, 101–106.

Brown, J.B., 1989. The Late Quaternary stratigraphy, paleohydrology, and geomorphology of pluvial Lake Mojave, Silver Lake and Soda Lake basins, southern California. Unpublished MS Thesis, University of Albuquerque, New Mexico, USA, 266p.

Brown, W.J., Rosen, M.R., 1995. Was there a Pliocene–Pleistocene fluvial–lacustrine connection between Death Valley and the Colorado River. Quaternary Research 43, 286–296.

Campbell, E.W.C., Campbell, W.E., Antevs, E., Amsden, C.A., Barbieri, J.A., Bode, F.D., 1937. The Archaeology of Lake Mojave: A Symposium in Southwest Museum Papers 11, Southwest Museum, Los Angeles, CA.

Enzel, Y., Cayan, D.R., Anderson, R., Wells, S.G., 1989. Atmospheric circulation during Holocene lake stands in the Mojave Desert: evidence of regional climate change. Nature 341, 44–47.

Enzel, Y., Knott, J.R., Anderson, K., Anderson, D.E., Wells, S.G., 2002. Is there evidence of Mega-Lake Manly in the Eastern Mojave Desert during Oxygen Isotope Stage 5e/6? A Comment on Hooke, R.L. (1999). Lake Manly(?) Shorelines in the Eastern Mojave Desert California, Quaternary Research 52, 328–336. Quaternary Research 57, 173–176.

Enzel, Y., Wells, S.G., Lancaster, N. (Eds.), 2003a. Paleoenvironments and paleohydrology of the Mojave and southern Great Basin Deserts. Geological Society of America Special Paper 368, Boulder CO, 249p.

Enzel, Y., Wells, S.G., Lancaster, N., 2003b. Late Pleistocene lakes along the Mojave River, southeast California. In: Enzel, Y., Wells, S.G., Lancaster, N. (Eds.), Paleoenvironments and Paleohydrology of the Mojave and Southern Great Basin Deserts. Geological Society of America Special Paper 368, Boulder, CO, pp. 61–77.

Evans, D.J.A., Benn, D.I., 2004. Facies descriptions and the logging of sedimentary exposures. In: Evans, D.J.A., Benn, D.I. (Eds.), A Practical Guide to the Study of Glacial Sediments. Arnold, London, pp. 11–50.

Farber, D.L., Hancock, G.S., Finkel, R.C., Rodbell, D.T., 2005. The age and extent of tropical alpine glaciation in the Cordillera Blanca, Peru. Journal of Quaternary Science 20, 759–776.

Forman, S.L., Pierson, J., 2002. Late Pleistocene luminescence chronology of loess deposition in the Missouri and Mississippi river valleys, United States. Paleogeography Paleoclimatology Paleoecology 186, 25–46.

Hu, Q., Feng, S., 2003. A daily soil temperature dataset and soil temperatature climatology of the contiguous United States. Journal of Applied Meteorology 42, 1139–1156.

Huntley, D.J., Lamothe, M., 2001. Ubiquity of anomalous fading in K-feldspars and the measurement and correction for it in optical dating. Canadian Journal of Earth Sciences 38, 1093–1106.

Ikeya, M., Ohmura, K., 1981. Dating of fossil shells with electron spin resonance. Journal of Geology 89, 247–251.

Jaiswal, M.K., 2005. Optically stimulated luminescence dating of fluvial sediments: applications and implications to paleoseismology and

paleoclimatology. Unpublished thesis submitted to M.S. University of Baroda, Vadodara, Gujarat, India.

Jefferson, G.T., 2003. Stratigraphy and paleontology of the middle to late Pleistocene Manix formation, and paleoenvironments of the central Mojave River, southern California. Geological Society of America Special Paper 368, 43–60.

Juyal, N., Pant, R.K., Basavaiah, N., Yadava, M.G., Saini, N.K., Singhvi, A.K., 2004. Climate and seismicity in the higher central Himalaya during the last 20–10 ka. Paleo3 213, 315–330.

Kaufman, D.S., 2000. Amino acid racemization in ostracodes. In: Goodfriend, G., Collins, M., Fogel, M., Macko, S., Wehmiller, J. (Eds.), Perspectives in Amino Acid and Protein Geochemistry. Oxford University Press, New York, pp. 145–160.

Kaufman, D.S., 2003. Amino acid paleothermometry of Quaternary ostracodes from the Bonneville Basin, Utah. Quaternary Science Reviews 22, 899–914.

Kaufman, D.S., Manley, W.F., 1998. A new procedure for determining enantiomeric (D/L) amino acid ratios in fossils using reverse phase liquid chromatography. Quaternary Science Reviews (Quaternary Geochronology) 17, 987–1000.

Kaufman, A., Broecker, W.S., Ku, T.-L., Thurber, D.L., 1971. The status of U-series methods of mollusc dating. Geochimica et Cosmochimica Acta 35, 1155–1183.

Kohl, C.P., Nishiizumi, K., 1992. Chemical isolation of quartz for measurement of in-situ-produced cosmogenic nuclides. Geochimica et Cosmochimica Acta 56, 3583–3587.

Lal, D., 1991. Cosmic ray labeling of erosion surfaces: in situ nuclide production rates and erosion models. Earth and Planetary Science Letters 104, 429–439.

Lang, A., 1994. Infrared stimulated luminescence dating of Holocene reworked silty sediments. Quaternary Science Reviews 13, 525–528.

Lang, A., Wagner, G.A., 1996. Infrared stimulated luminescence dating of archaeosediments. Archaeometry 38, 129–141.

Lin, J.C., Broecker, W.S., Anderson, R.F., Hemming, S., Rubenstone, J.L., Bonani, G., 1996. New ^{230}Th/U and ^{14}C ages from Lake Lahontan carbonates, Nevada, USA, and a discussion of the origin of initial thorium. Geochimica et Cosmochimica Acta 60, 2817–2832.

Mejdahl, V., 1979. Thermoluminescence dating: beta attenuation in quartz grains. Archaeometry 21, 61–73.

Miller, G.H., Brigham-Grette, J., 1989. Amino acid geochronology—resolution and precision in carbonate fossils. Quaternary International 1, 111–128.

Murray, A.S., Wintle, A.G., 2000. Luminescence dating of quartz using an improved single-aliquot regenerative-dose protocol. Radiation Measurements 32, 57–73.

Nishiizumi, K., 2004. Preparation of ^{26}Al AMS standards. Nuclear Instruments and Methods in Physics Research B 223–224, 388–392.

Nishiizumi, K., Kohl, C.P., Arnold, J.R., Dorn, R., Klein, J., Fink, D., Middleton, R., 1993. Role of in situ cosmogenic nuclides ^{10}Be and ^{26}Al in the study of diverse geomorphic processes. Earth Surface Processes and Landforms 18, 407–425.

Ore, H.T., Warren, C.N., 1971. Late Pleistocene–Early Holocene geomorphic history of Lake Mojave, California. Geological Society of America Bulletin 82, 2553–2562.

Prescott, J.R., Hutton, J.T., 1994. Cosmic ray contributions to dose rates for luminescence and ESR dating. Large depths and long-term time variations. Radiation Measurements 23, 497–500.

Radtke, U., Hennig, G.J., Linke, W., Müngersdorf, J., 1981. Th-230/U-234 and ESR- dating of fossil shells in Pleistocene marine terraces (Northern Latium, Central Italy). Quaternaria 23, 37–50.

Reimer, P.J., Baillie, M.G.L., Bard, E., Bayliss, A., Beck, J.W., Bertrand, C.J.H., Blackwell, P.G., Buck, C.E., Burr, G.S., Cutler, K.B., Damon, P.E., Edwards, R.L., Fairbanks, R.G., Friedrich, M., Guilderson, T.P., Hogg, A.G., Hughen, K.A., Kromer, B., McCormac, G., Manning, S., Ramsey, C.B., Reimer, R.W., Remmele, S., Southon, J.R., Stuiver, M., Talamo, S., Taylor, F.W., van der Plicht, J., Weyhenmeyer, C.E., 2004. IntCal04 terrestrial radiocarbon age calibration, 0–26 cal kyr BP. Radiocarbon 46, 1029.

Rendell, H.M., Townsend, P.D., Wood, R.A., 1995. TL and IRSL emission-spectra of detrital feldspars. New Experimental-Data. Physica Status Solidi B-Basic Research 190, 321–330.

Richardson, C.A., McDonald, E.V., Busacca, A.J., 1997. Luminescence dating of loess from the northwest United States. Quaternary Science Reviews 16 (3–5), 403–415.

Schellmann, G., Radtke, U., 1999. Problems encountered in the determination of dose and dose rate in ESR dating of mollusc shells. Quaternary Science Reviews 18, 1515–1527.

Schellmann, G., Radtke, U., 2001. Progress in ESR dating of young and middle Quaternary Corals. Quaternary Science Reviews 20, 1015–1020.

Sharp, W.D., Ludwig, K.R., Chadwick, O.A., Amundson, R., Glaser, L.L., 2003. Dating fluvial terraces by ^{230}Th/U on pedogenic carbonate, Wind River Basin, Wyoming. Quaternary Research 59, 139–150.

Singhvi, A.K., 2007. Luminescence dating: an example of synergistic mutualism between Geology and Physics. In: Selvasekaranpandian, S., Murthy, K.V.R., Natarajan, V., Malathi, J., Brahmanandhan, G.M., Khanna, D. (Eds.), Luminescence and its Applications. McMillan India Ltd., Bangalore, pp. 6–10.

Singhvi, A.K., Sharma, Y.P., Agrawal, D.P., 1982. Thermo-luminescence dating of sand dunes in Rajasthan, India. Nature 295, 313–315.

Spooner, N.A., Aitken, M.J., Smith, B.W., Franks, M., McElroy, C., 1990. Archaeological dating by infrared-stimulated luminescence using a diode-array. Radiation Protection Dosimetry 34 (1–4), 83–86.

Stone, J.O., 2000. Air pressure and cosmogenic isotope production. Journal of Geophysical Research 105, 23,753–23,759.

Stuiver, M., Polach, H., 1977. Reporting of ^{14}C data. Radiocarbon 19, 355–363.

Thompson, G.D., 1921. Pleistocene lakes along the Mojave River, California. Journal of the Washington Academy of Sciences 11, 423–424.

Thompson, G.D., 1929. The Mojave Desert region, California: a geographic, geologic and hydrological reconnaissance. US Geological Survey Water-Supply Paper 578, 1–143 and 371–572.

Warren, C.N., Ore, H.T., 1978. Approach and process of dating Lake Mojave artifacts. The Journal of California Archaeology 5, 179–187.

Warren, C.N., Ore, H.T., 2004a. Data recovery at site CA-SBR-6566. In: Blair, L.M., Wedding, J.R., Rose, S.F., Smith, A.J. (Eds.), Kern River 2003 Expansion Project: California, vol. 2. Cultural Resources Data Recovery Report. Harry Reid Center for Environmental Studies HRC Report 5-150-14 [29]. University of Nevada, Las Vegas, pp. 135–138.

Warren, C.N., Ore, H.T., 2004b. Data recovery at site CA-SBR-140. In: Blair, L.M., Wedding, J.R., Rose, S.F., Smith, A.J. (Eds.), Kern River 2003 Expansion Project: California, vol. 2. Cultural Resources Data Recovery Report. Harry Reid Center for Environmental Studies HRC Report 5-150–14 [29]. University of Nevada, Las Vegas, pp. 79–117.

Wehmiller, J.F., 1977. Amino acid studies of the Del Mar, California, midden site—apparent rate constants, ground temperature models, and chronological implications. Earth and Planetary Science Letters 37, 184–196.

Wehmiller, J.F., Stecher III, H.A., York, L.L., Friedman, I., 2000. The thermal environment of fossils: effective ground temperatures at aminostratigraphic site on the US Atlantic Coastal Plain. In: Goodfriend, G., Collins, M., Fogel, M., Macko, S., Wehmiller, J. (Eds.), Perspectives in Amino Acid and Protein Geochemistry. Oxford University Press, New York, pp. 219–252.

Wells, S.G., Brown, W.J., Enzel, Y., Anderson, R.Y., McFadden, L.D., 2003. Late Quaternary geology and paleohydrology of pluvial Lake Mojave, southern California. Geological Society of America Special Paper 368, 79–114.